NATIONAL ADVISORY COMMITTEE FOR AERONAUTICS

TECHNICAL NOTE 3814

EFFECTS OF VERTICAL FINS NEAR THE NOSE OF THE FUSELAGE ON THE DIRECTIONAL AND DAMPING-IN-YAW STABILITY DERIVATIVES OF AN AIRPLANE MODEL UNDER STEADY-STATE AND OSCILLATORY CONDITIONS

By M. J. Queijo and Evalyn G. Wells

Langley Aeronautical Laboratory
Langley Field, Va.

Washington
December 1956

NATIONAL ADVISORY COMMITTEE FOR AERONAU.

TECHNICAL NOTE 3814

EFFECTS OF VERTICAL FINS NEAR THE NOSE OF THE FUSELAGE ON THE DIRECTIONAL AND DAMPING-IN-YAW STABILITY DERIVATIVES OF AN AIRPLANE MODEL UNDER STEADY-STATE AND OSCILLATORY CONDITIONS

By M. J. Queijo and Evalyn G. Wells

SUMMARY

An experimental investigation has been made to determine the effects of vertical fins near the nose of the fuselage on the directional and damping-in-yaw stability derivatives of a swept-wing airplane model. The investigation included measurements of these characteristics for the model oscillating about a vertical axis in a steady airstream.

The results of this investigation showed that, for angles of attack up to at least 12°, fins placed above the fuselage nose decreased the directional stability but increased the damping in yaw of the model in both the steady-state and oscillatory conditions because of the sidewash acting on the tail as well as the direct lift of the fins. Also, fins placed above the fuselage nose were more effective in increasing the steady-state or oscillatory damping in yaw than the addition of an equal amount of area at the vertical tail.

Fins placed below the nose of the fuselage decreased the directional stability and increased the damping in yaw to a lesser extent than fins placed above the fuselage nose in the steady-state condition but reduced the damping in yaw in the oscillatory condition. For a constant value of directional stability, the damping in yaw could be greatly increased by the use of a fin placed above the nose of the fuselage and an increase in tail size.

INTRODUCTION

Some of the present-day high-speed airplanes have shown poor damping of the lateral oscillation. This situation has led to renewed consideration of methods for improving the lateral damping. One of the methods

under consideration involves the use of vortex generators located ahead of the vertical tail. This method takes advantage of the lag of the sidewash at the vertical tail due to the vortex generator. (See ref. 1, for example.) The investigation in reference 1 was concerned with two methods of varying the sidewash at the vertical tail: varying the wing height and using vertical fins with their aerodynamic centers located over the assumed center-of-gravity position of the airplane model. This fin position was chosen in order to minimize the loss in directional stability while generating the desired sidewash.

The present investigation is also concerned with the use of vertical fins for improving the damping in yaw. In this investigation, however, the vertical fins were located ahead of the assumed center-of-gravity position of the model. Simple geometric considerations show that this fin position should increase the damping in yaw because of the direct lift on the fins as well as the sidewash at the vertical tail. Since both of these factors also tend to reduce the directional stability, the vertical-tail size was increased for use with some of the fins in order to maintain directional stability.

Results were obtained under conditions of steady-state sideslipping, steady-state yawing, and with the model oscillating about a vertical axis.

SYMBOLS

The data presented herein are referred to the stability system of axes with the origin at the projection of the quarter chord of the wing mean aerodynamic chord on the plane of symmetry. (See fig. 1.) The symbols and coefficients are defined as follows:

b	wing span, ft
b_v	vertical-tail span, ft
b_f	vertical-fin span, ft
c	chord, ft
$\bar{c}$	mean aerodynamic chord, $\frac{2}{S}\int_0^{b/2} c^2 dy$, ft
f	frequency, cps
F_1, F_2, F_3, F_4	designations of vertical fin used

F_Y lateral force, lb

I_Z moment of inertia about vertical axis, slug-ft^2

k reduced-frequency parameter, $\frac{\omega b}{2V}$

M_X rolling moment, ft-lb

M_Z yawing moment, ft-lb

K mechanical spring constant, ft-lb/radians

q dynamic pressure, $\frac{1}{2}\rho V^2$, lb/sq ft

$r,\dot{\psi}$ yawing velocity, $\frac{d\psi}{dt}$, radians/sec

$\dot{r},\ddot{\psi}$ yawing acceleration, $\frac{d^2\psi}{dt^2}$, radians/sec^2

S wing area, sq ft

S_o exposed area (outside of fuselage) of basic vertical tail V_1

S_e total exposed area of vertical tail and fin

t time, sec

$t_{1/2}$ time required for lateral oscillation to damp to half-amplitude, sec

V free-stream velocity, ft/sec

V_1,V_2,V_3,V_4 designations of vertical tail used

X,Y,Z stability axes

$\bar{x},\bar{z}$ distances from leading-edge root chord to center of pressure of vertical tail or fin

α angle of attack of fuselage center line, deg

β angle of sideslip, deg unless otherwise specified ($\beta = -\psi$ for these tests)

$\dot{\beta} = \frac{\partial \beta}{\partial t}$

σ sidewash angle, radians

ρ mass density of air, slugs/cu ft

ψ angle of yaw, radians

ω circular frequency of oscillation, radians/sec

C_L lift coefficient, $\frac{\text{Lift}}{qS}$

C_l rolling-moment coefficient, $\frac{M_X}{qSb}$

$C_{l_\beta} = \frac{\partial C_l}{\partial \beta}$

$C_{l_r} = \frac{\partial C_l}{\partial \left(\frac{rb}{2V}\right)}$

C_n yawing-moment coefficient, $\frac{M_Z}{qSb}$

$C_{n_\beta} = \frac{\partial C_n}{\partial \beta}$

$C_{n_{\dot{\beta}}} = \frac{\partial C_n}{\partial \left(\frac{\dot{\beta} b}{2V}\right)}$

$C_{n_r} = \frac{\partial C_n}{\partial \left(\frac{rb}{2V}\right)}$

$C_{n_{\dot{r}}} = \frac{\partial C_n}{\partial \left(\frac{\dot{r} b^2}{4V^2}\right)}$

C_Y lateral-force coefficient, $\frac{F_Y}{qS}$

$$C_{Y_\beta} = \frac{\partial C_Y}{\partial \beta}$$

$$C_{Y_r} = \frac{\partial C_Y}{\partial \left(\frac{rb}{2V}\right)}$$

Subscripts:

F	fin
l	indicates fin below fuselage center line
r	root
t	tip
u	indicates fin above fuselage center line
V	vertical tail
ω	indicates a derivative measured during an oscillation test

Dots over a symbol indicate the derivatives of the quantity with respect to time.

MODEL AND APPARATUS

A photograph of the model used in the investigation is given as figure 2 and a drawing of the model with all pertinent dimensions is given in figure 3. Four vertical tails and four fins were used, and their dimensions are given in figures 4 and 5, respectively. All tails and fins were constructed of 1/2-inch plywood and had rounded leading edges and beveled trailing edges. The tails and fins were mounted on the fuselages so that the distances from their estimated aerodynamic centers to the assumed model center of gravity were 1.20b/2 and 1.50b/2, respectively.

All tests were made in the 6- by 6-foot test section of the Langley stability tunnel. The steady-state tests were made with the model mounted on a single strut support. The steady-state yawing tests were made by using the curved-flow technique of the Langley stability tunnel, which consists of curving the airstream about a stationary model.

The apparatus described in reference 2 was used to measure the directional stability and damping in yaw of the model under oscillatory conditions. The model was mounted on a strut which was free to oscillate in yaw. Restoring moments were provided by flexures, which supported the oscillatory strut, and also by a torque rod. A mirror clamped to a section of the strut which extended outside the tunnel reflected a beam of light into an optical recorder. A continuous record of the motion of the model, after an initial displacement in yaw, was obtained on film. A timer in the recorder exposed timing lines on the film in order that time, as well as model displacement, could be determined.

TESTS

Force Tests

All model configurations were tested through an angle-of-attack range from about -4° to 28° at sideslip angles of 0° and $\pm 5^\circ$. The static sideslip derivatives C_{Y_β}, C_{l_β}, and C_{n_β} were obtained from the data at $\pm 5^\circ$ sideslip.

The steady-yawing derivatives C_{Y_r}, C_{l_r}, and C_{n_r} were obtained by use of the standard curved-flow technique of the Langley stability tunnel at tunnel-wall curvatures corresponding to values of $\frac{rb}{2V}$ of 0, -0.0336, -0.0711, and -0.0936 and for angles of attack from about -4° to 28°.

Oscillation Tests

The oscillation tests were made at angles of attack of 0°, 6°, and 12° and consisted of deflecting the model 7° in yaw and then releasing it. The resulting motion was allowed to damp to less than one-half its original amplitude while a continuous record of the amplitude of the motion and time was obtained. The period of oscillation of the model with vertical tail V_1 and no fins was about 0.9 second which for these tests corresponds to a value of $\frac{\omega b}{2V}$ of 0.06.

The range of reduced frequencies obtained with the other configurations varied from 0.02 to about 0.08. (See table I.) Some investigations have shown that reduced frequency can have a large effect on certain oscillatory derivatives. No attempt was made in the present investigation to obtain particular values of reduced frequency for model configurations other than the basic configuration (with V_1) on the basis that the purpose herein was to determine the effects of adding fins and changing tail size,

both of which change reduced frequency. It should be remembered, therefore, that comparisons of data on some other basis (for example, all data obtained at the same reduced frequency) might lead to comparisons and conclusions different from those obtained in the present investigation.

All tests were made at a dynamic pressure of 24.9 pounds per square foot, which corresponds to a Mach number of 0.13 and a Reynolds number of 0.87×10^6 based on the wing mean aerodynamic chord.

Reduction of Test Data

The time required for the amplitude of motion of each model configuration to damp to half-amplitude and the period of the oscillation were measured from the continuous film record. The measurements were made at the large amplitudes of motion in order to minimize effects of tunnel turbulence on the model motion. The oscillatory damping in yaw and directional stability were computed from the following expressions of reference 2:

$$C_{n_{r,\omega}} - C_{n_{\dot{\beta},\omega}} = -\frac{2.772VI_Z}{qSb^2}\left[\left(\frac{1}{t_{1/2}}\right)_{\text{wind on}} - \left(\frac{1}{t_{1/2}}\right)_{\text{wind off}}\right]$$

$$C_{n_{\beta,\omega}} + k^2 C_{n_{\dot{r},\omega}} = \frac{1}{qSb}\left[I_Z(2\pi f)^2 + K\right]$$

The term K represents the spring constant of the flexures and torque rod and was 28.7 foot-pounds/radian for these tests.

RESULTS AND DISCUSSION

The parameters C_{Y_β}, C_{l_β}, C_{n_β}, C_{Y_r}, C_{l_r}, and C_{n_r} were measured in the steady-state tests, and the parameters $C_{n_{\beta,\omega}} + k^2 C_{n_{\dot{r},\omega}}$ and $C_{n_{r,\omega}} - C_{n_{\dot{\beta},\omega}}$ were measured in the oscillation tests. Since the investigation was concerned primarily with directional stability and damping in yaw, the discussion is limited to the parameters C_{n_β}, C_{n_r}, $C_{n_{\beta,\omega}} + k^2 C_{n_{\dot{r},\omega}}$, and $C_{n_{r,\omega}} - C_{n_{\dot{\beta},\omega}}$. As stated previously the steady-state sideslip derivatives were obtained from data at $\beta = \pm 5^\circ$. If any nonlinearities in the curves of the data plotted against β occur within this range, the forces and moments indicated by C_{n_β}, C_{Y_β}, and C_{l_β} are applicable only at $\beta = \pm 5^\circ$.

The basic data obtained in this investigation are plotted against angle of attack. Figure 6 is a plot of C_L against α for the model and can be used to relate the data to the lift coefficient.

Steady-State Results

Sideslip derivatives.- The steady-state sideslip derivatives C_{Y_β}, C_{l_β}, and C_{n_β} are plotted against angle of attack in figures 7 to 10 for the various model configurations. Addition of vertical fins near the nose of the fuselage decreased the directional-stability parameter C_{n_β} for all configurations for angles of attack up to about 20°. In this angle-of-attack range the addition of a fin above the fuselage center line reduced C_{n_β} more than the addition of a fin of equal size below the fuselage center line for all configurations tested. This is attributable to the fact that either fin contributes some instability because of its lift; however, the sidewash from the upper fin also reduces the vertical-tail effectiveness. Addition of fins both above and below the fuselage center line caused a decrease in C_{n_β} which was very nearly equal to the sum of the changes obtained by adding the upper and lower fins individually. At high angles of attack (above 20°) some of the lower fins contributed a large positive increment in C_{n_β}.

Some of the data of figures 7 to 10 are replotted in figure 11 to show the relative effects of adding area to the vertical tail or as a fin near the nose of the fuselage. The results are given for angles of attack up to 12° as curves of C_{n_β} plotted against the area ratio S_e/S_o, which is the ratio of total tail and fin exposed area to the exposed area of vertical tail V_1. The dashed line shows the variation in C_{n_β} obtained by increasing the vertical-tail size. The solid lines show the change in C_{n_β} obtained by adding fins to the model with the various vertical tails. These results show, perhaps a little more clearly, the decrease in C_{n_β} caused by the addition of fins near the nose of the fuselage and also show that the decrease in C_{n_β} with added fin area becomes greater with increase in angle of attack.

Yawing derivatives.- The steady-state yawing derivatives C_{Y_r}, C_{l_r}, and C_{n_r} for the various model configurations are presented in figures 12 to 15. Addition of a fin above or below the fuselage center line increased the damping in yaw for angles of attack up to about 20°. Fins above the fuselage center line caused a greater increase in damping than did fins of the same size below the fuselage center line. This is due

to the fact that for yawing flight the sidewash from the fins increases the damping in yaw, and the vertical tail is more directly in the sidewash field of the upper fins than of the lower fins throughout most of the angle-of-attack range tested. At high angles of attack (above 20°) some of the lower fins decreased the damping in yaw of the model.

Part of the data of figures 12 to 15 are replotted in figure 16 as curves of C_{n_r} against the area ratio S_e/S_o. These data show that the addition of area as a fin caused a greater increase in damping than the addition of an equal amount of tail area and that the upper fin is much more effective in increasing the damping than a lower fin of equal size. Both of these trends increase with angle of attack up to at least 12°.

The data of figures 11 and 16 are cross-plotted in figure 17 to show corresponding values of C_{n_r} and C_{n_β} for the various tail-fin combinations. This figure shows that any particular combination of C_{n_r} and C_{n_β} can be obtained by proper choice of tail and fin; however, for a given tail a smaller fin is required if it is placed above the fuselage center line than would be required if it were placed below the fuselage center line. Also, the damping in yaw of the basic model can be greatly increased while the directional stability C_{n_β} is kept constant by properly adding area at the tail and as a nose fin. For example, at $\alpha = 6.4°$, the value of C_{n_r} of the model with vertical tail V_1 is -0.56 and C_{n_β} is 0.215. The damping-in-yaw parameter C_{n_r} can be almost doubled while C_{n_β} is kept constant by increasing the exposed vertical-tail area by 60 percent (to obtain V_3) and adding an upper fin having an exposed area of 15 percent of that of tail V_1.

Oscillatory Results

Sideslip derivatives.- The sideslip derivatives measured during the oscillation tests are presented in figure 18 as curves of $C_{n_{\beta,\omega}} + k^2 C_{n_{\dot{r}},\omega}$ plotted against the area ratio S_e/S_o. The results are similar to those obtained under steady-state conditions (fig. 11) and indicate that the term $k^2 C_{n_{\dot{r}},\omega}$ is small.

Yawing derivatives.- The yawing derivatives measured during the oscillation tests are presented in figure 19 as curves of the damping-in-yaw parameter $C_{n_{r,\omega}} - C_{n_{\dot{\beta}},\omega}$ plotted against the area ratio S_e/S_o for the various model configurations. The results are generally similar to those obtained in the steady-state tests (except for the lower fin data) and show that for any particular tail size the addition of a vertical fin above the fuselage center line generally increased the damping in yaw and that the increase was greater than that obtained by adding an

equal area at the vertical tail. Both of these trends increased with increase in angle of attack to $\alpha = 12^\circ$. In general, fins placed below the fuselage center line decreased the oscillatory damping in yaw.

A comparison of figures 16 and 19 shows that the oscillatory damping in yaw was greater than the steady-state damping for all configurations tested. This may be largely attributable to the effect of the lag of the sidewash (discussed in ref. 1) which increases the oscillatory damping over the steady-state damping by the factor $1 - \frac{\partial \sigma}{\partial \beta}$. The large oscillatory damping for the model with vertical fins was caused by the large sidewash generated by the fins. The increase in oscillatory damping over the steady-state damping for the model with no fins may be associated with the dihedral and incidence of the wing or vortex flow from the fuselage.

The damping-in-yaw parameter $C_{n_{r,\omega}} - C_{n_{\dot{\beta},\omega}}$ is plotted against the directional-stability parameter $C_{n_{\beta,\omega}} + k^2 C_{n_{\dot{r},\omega}}$ in figure 20 to show corresponding values of the two parameters for the various configurations tested. The trends shown are similar to those for the steady-state data (except for the lower tail as noted previously) even though the results are somewhat more erratic than those for the steady-state results.

CONCLUSIONS

An experimental investigation has been made to determine the effects of vertical fins near the fuselage nose on the directional stability and damping-in-yaw characteristics of a swept-wing airplane model. The investigation included measurements of these characteristics for the model oscillating about a vertical axis in a steady airstream. The results of the investigation have led to the following conclusions which apply up to angles of attack of at least 12°:

1. The damping in yaw of the model could be increased under steady-state or oscillatory conditions by use of fins placed above the fuselage center line, and this trend increased with increase in angle of attack. This effect is attributable to the sidewash from the fins acting on the tail as well as to the direct lift on the fins.

2. Fins placed above the fuselage center line were more effective in increasing either the steady-state or the oscillatory damping in yaw than the addition of an equal amount of area at the vertical tail.

3. Fins below the fuselage center line increased the steady-state damping in yaw but not as much as did fins above the fuselage center line. Under oscillatory conditions, fins below the fuselage center line decreased the damping in yaw.

4. Fins placed either above or below the fuselage center line decreased the directional stability of the model under steady-state or oscillatory conditions. Fins above the fuselage center line, however, caused a greater decrease than did fins of equal size below the fuselage center line.

5. The damping in yaw of the model could be greatly increased for a constant value of directional stability by the use of an upper fin and an increase in tail size.

Langley Aeronautical Laboratory,
National Advisory Committee for Aeronautics,
Langley Field, Va., June 27, 1956.

REFERENCES

1. Fisher, Lewis R., and Fletcher, Herman S.: Effect of Lag of Sidewash on the Vertical-Tail Contribution to Oscillatory Damping in Yaw of Airplane Models. NACA TN 3356, 1955.

2. Bird, John D., Fisher, Lewis R., and Hubbard, Sadie M.: Some Effects of Frequency on the Contribution of a Vertical Tail to the Free Aerodynamic Damping of a Model Oscillating in Yaw. NACA Rep. 1130, 1953. (Supersedes NACA TN 2657.)

TABLE I.- REDUCED-FREQUENCY PARAMETER FOR THE VARIOUS MODEL CONFIGURATIONS

Configuration	Reduced-frequency parameter $\omega b/2V$ for -		
	$\alpha = 0°$	$\alpha = 6°$	$\alpha = 12°$
V_1	0.064	0.064	0.067
$V_1 + F_{1,u}$	.057	.047	.045
$V_1 + F_{1,l}$	.061	.062	.065
V_2	.070	.070	.074
$V_2 + F_{1,u}$	.064	.056	.053
$V_2 + F_{1,l}$	.068	.070	.069
$V_2 + F_{1,u} + F_{1,l}$	.060	.050	.048
$V_2 + F_{2,u}$	.049	.032	.030
$V_2 + F_{2,l}$	.060	.063	.066
V_3	.078	.077	.080
$V_3 + F_{1,u}$	.072	.065	.060
$V_3 + F_{1,l}$	.075	.075	.078
$V_3 + F_{1,u} + F_{1,l}$	.070	.061	.058
$V_3 + F_{2,u}$	.060	.047	.037
$V_3 + F_{2,l}$	.068	.068	.073
$V_3 + F_{3,u}$	.054	.036	.030
$V_3 + F_{3,l}$	.065	.064	.067
$V_3 + F_{4,u}$	.045	.027	.023
$V_3 + F_{4,l}$	.062	.061	.064
V_4	.082	.082	.084
$V_4 + F_{1,u}$	.075	.069	.070
$V_4 + F_{1,l}$	.080	.079	.083
$V_4 + F_{1,u} + F_{1,l}$	.074	.066	.069
$V_4 + F_{2,u}$	.067	.053	.048
$V_4 + F_{2,l}$	.074	.073	.080
$V_4 + F_{2,u} + F_{2,l}$	.053	.039	.047
$V_4 + F_{3,u}$	.059	.041	.040
$V_4 + F_{3,l}$	.069	.069	.074
$V_4 + F_{4,u}$	.054	.038	.039
$V_4 + F_{4,l}$	.069	.067	.070

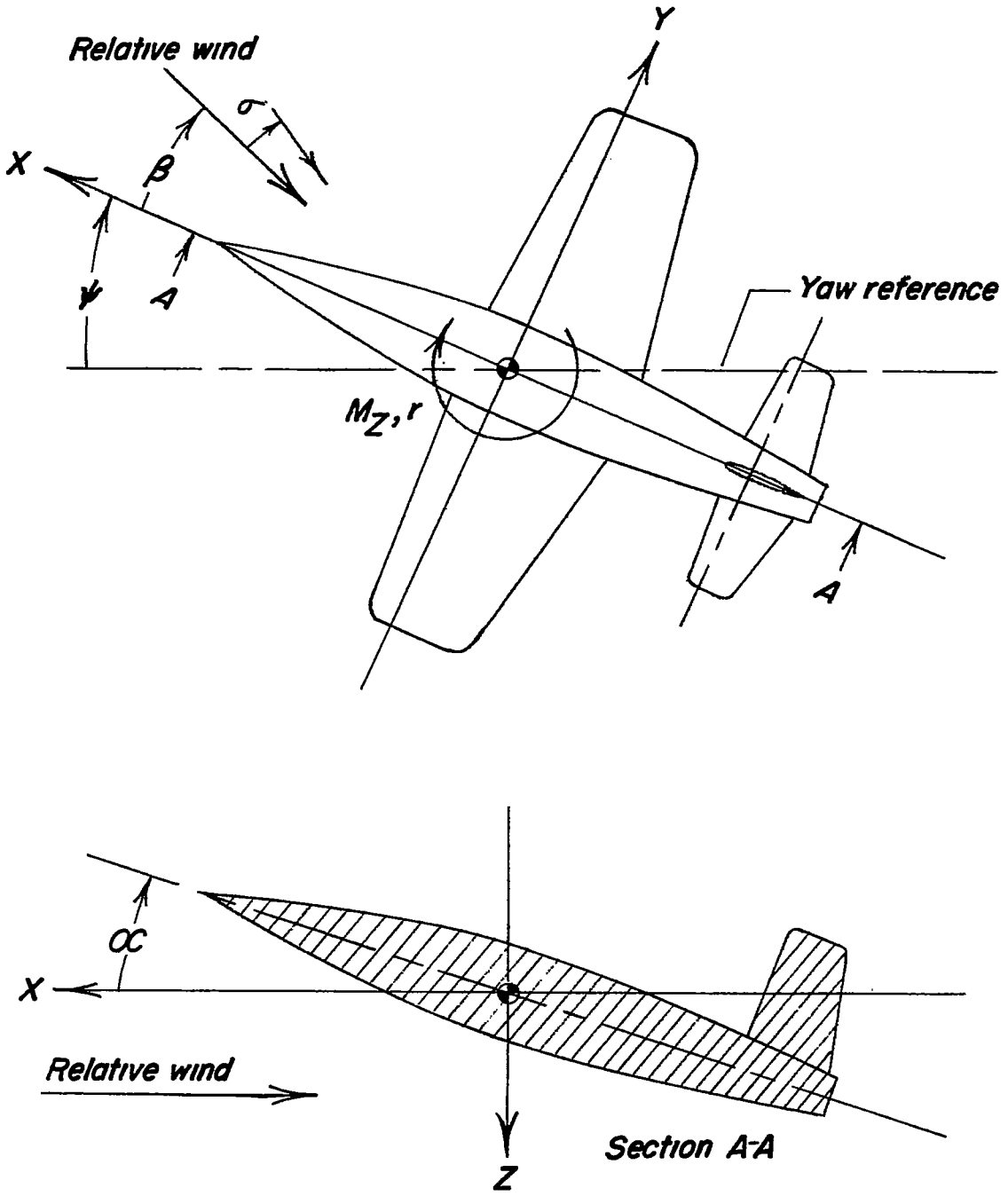

Figure 1.- System of stability axes. Arrows indicate positive forces, moments, and angular displacements. Yaw reference is generally chosen to coincide with initial relative wind.

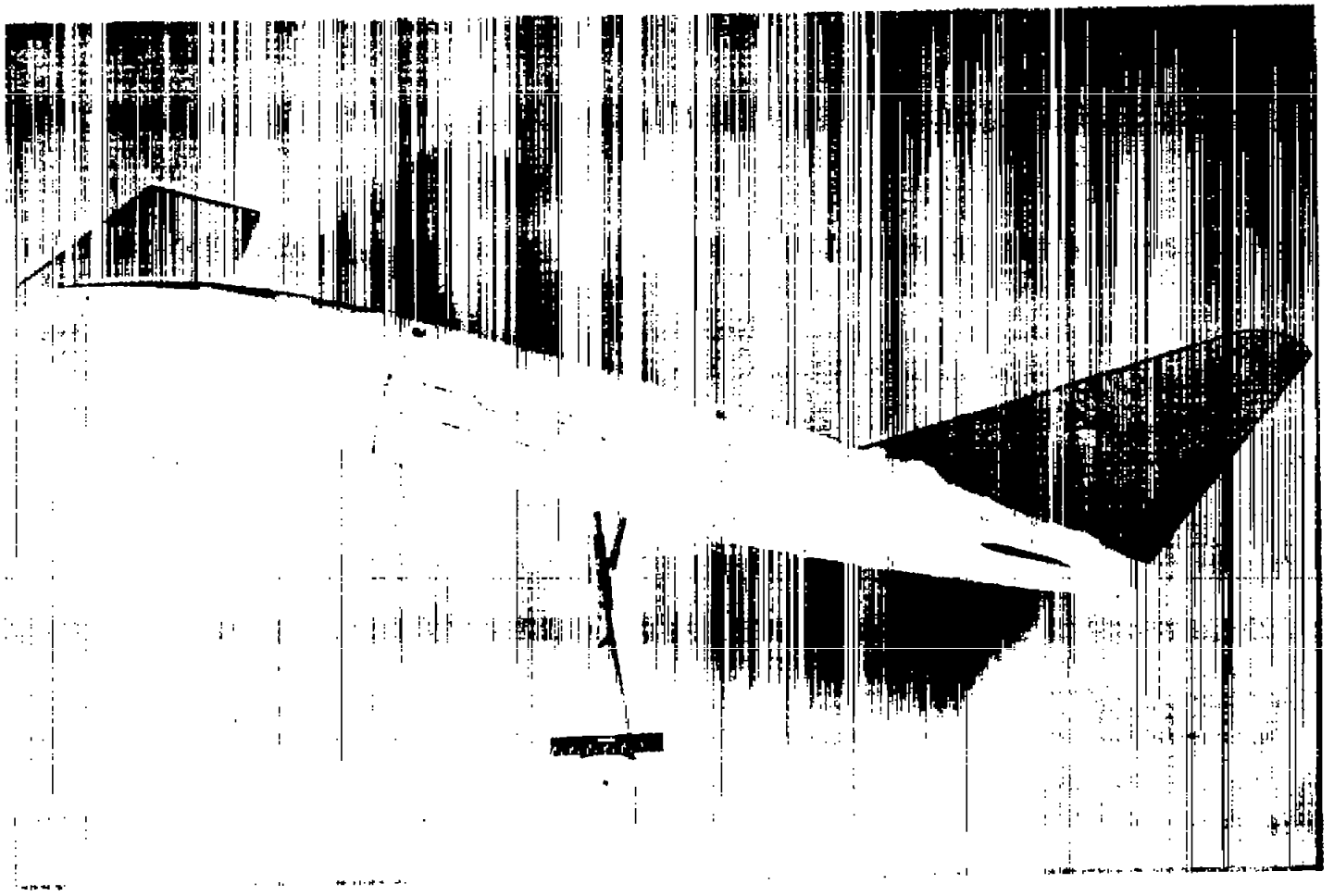

L-93227.1

Figure 2.- Photograph of model used in the investigation. $V_3 + F_{3,u} + F_{3,l}$.

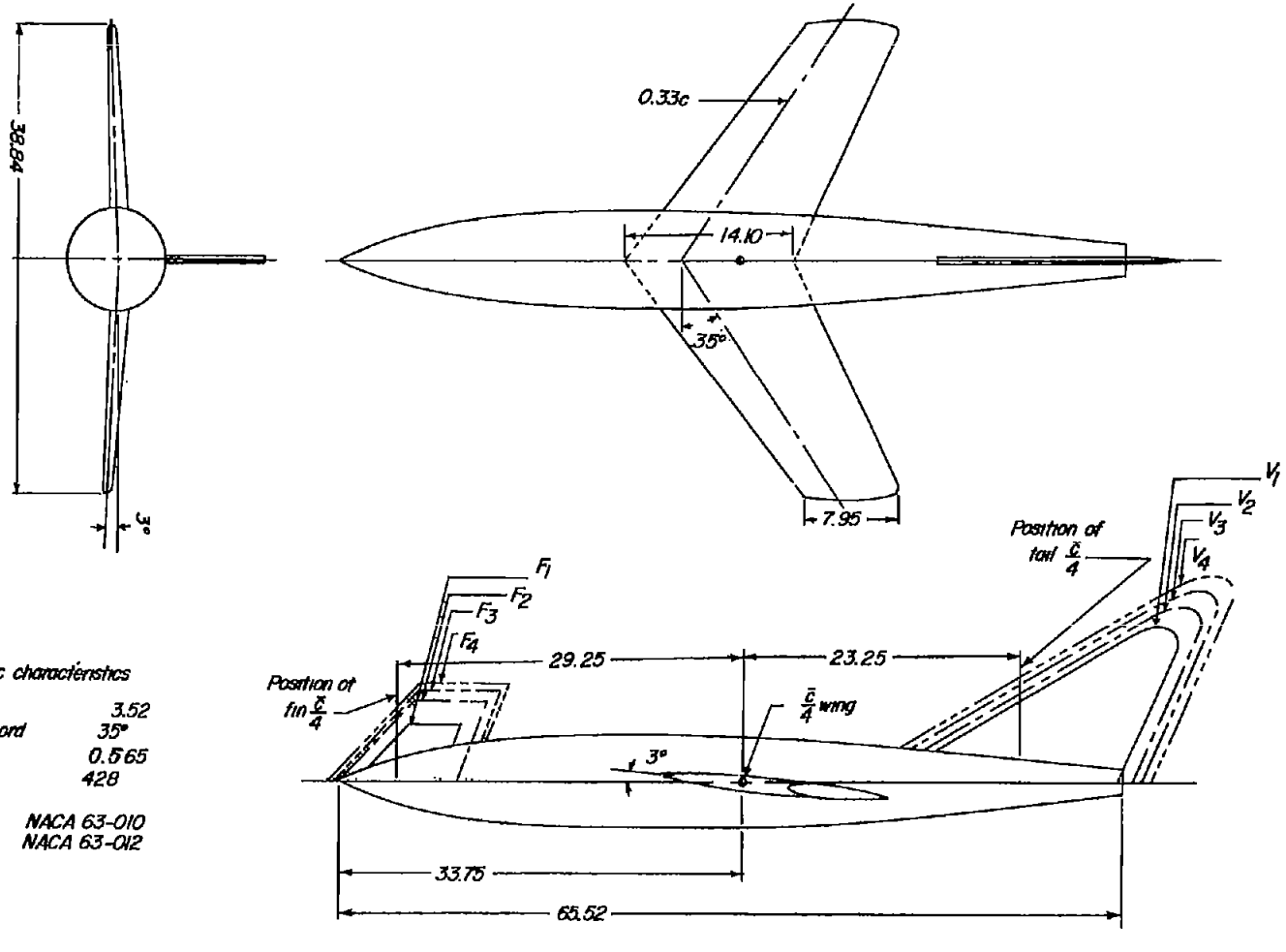

Wing geometric characteristics

Aspect ratio	3.52
Sweep of 0.33 chord	35°
Taper ratio	0.565
Area, sq in.	428
Airfoil	
Root	NACA 63-010
Tip	NACA 63-012

Figure 3.- Drawing of model used in the investigation. All dimensions are in inches.

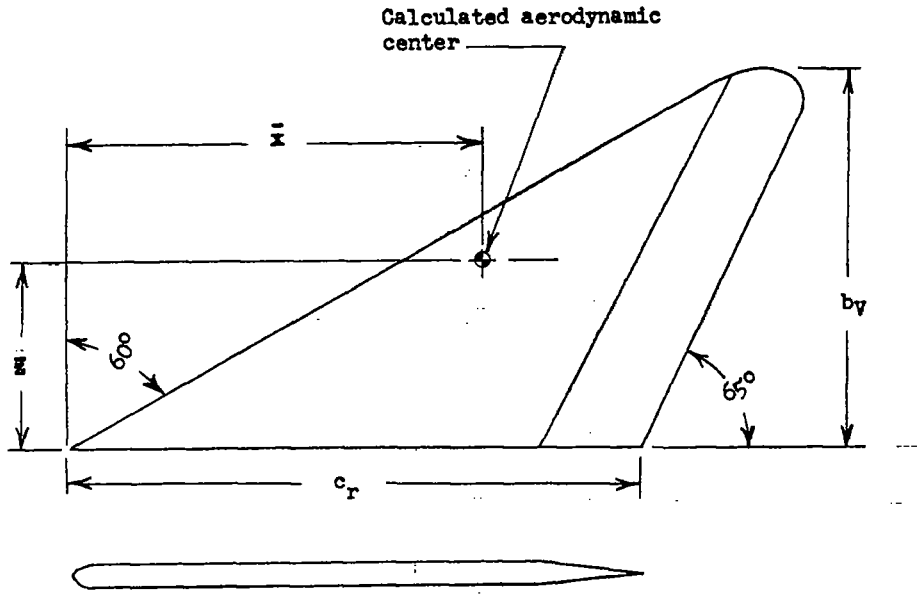

Vertical tail	b_V, in.	c_r, in.	$\bar{x}$, in.	$\bar{z}$, in.	Total tail area, sq in.	Exposed tail area, sq in.	Exposed tail area / Total wing area
V_1	12.68	18.90	10.95	4.28	148	107	.25
V_2	14.15	21.10	12.26	4.78	184	140	.35
V_3	15.50	23.10	13.43	5.26	221	173	.40
V_4	16.75	25.00	14.48	5.65	258	206	.48

Figure 4.- Vertical-tail geometric characteristics.

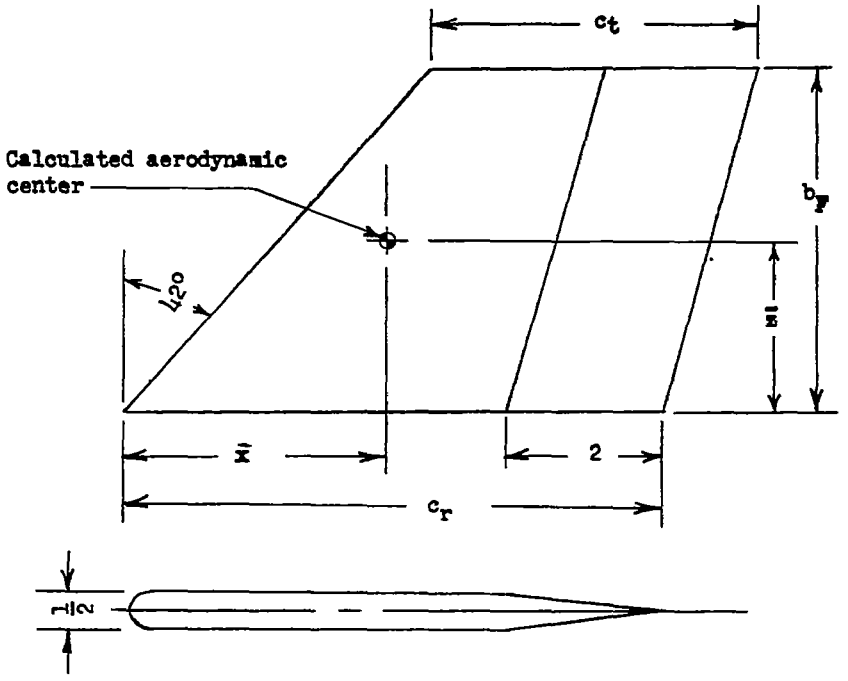

Fin	b_F, in.	c_t, in.	c_r, in.	$\bar{x}$, in.	$\bar{z}$, in.	Total fin area, sq in.	Exposed fin area, sq in.	Exposed fin area / Total wing area
F_1	4.59	4.24	7.07	3.32	2.30	27.0	12.3	.028
F_2	6.50	6.00	10.00	4.70	3.25	52.0	33.1	.077
F_3	7.26	6.70	11.18	5.26	3.63	65.0	44.1	.103
F_4	7.96	7.35	12.20	5.74	3.98	79.0	55.4	.129

Figure 5.- Fin geometric characteristics.

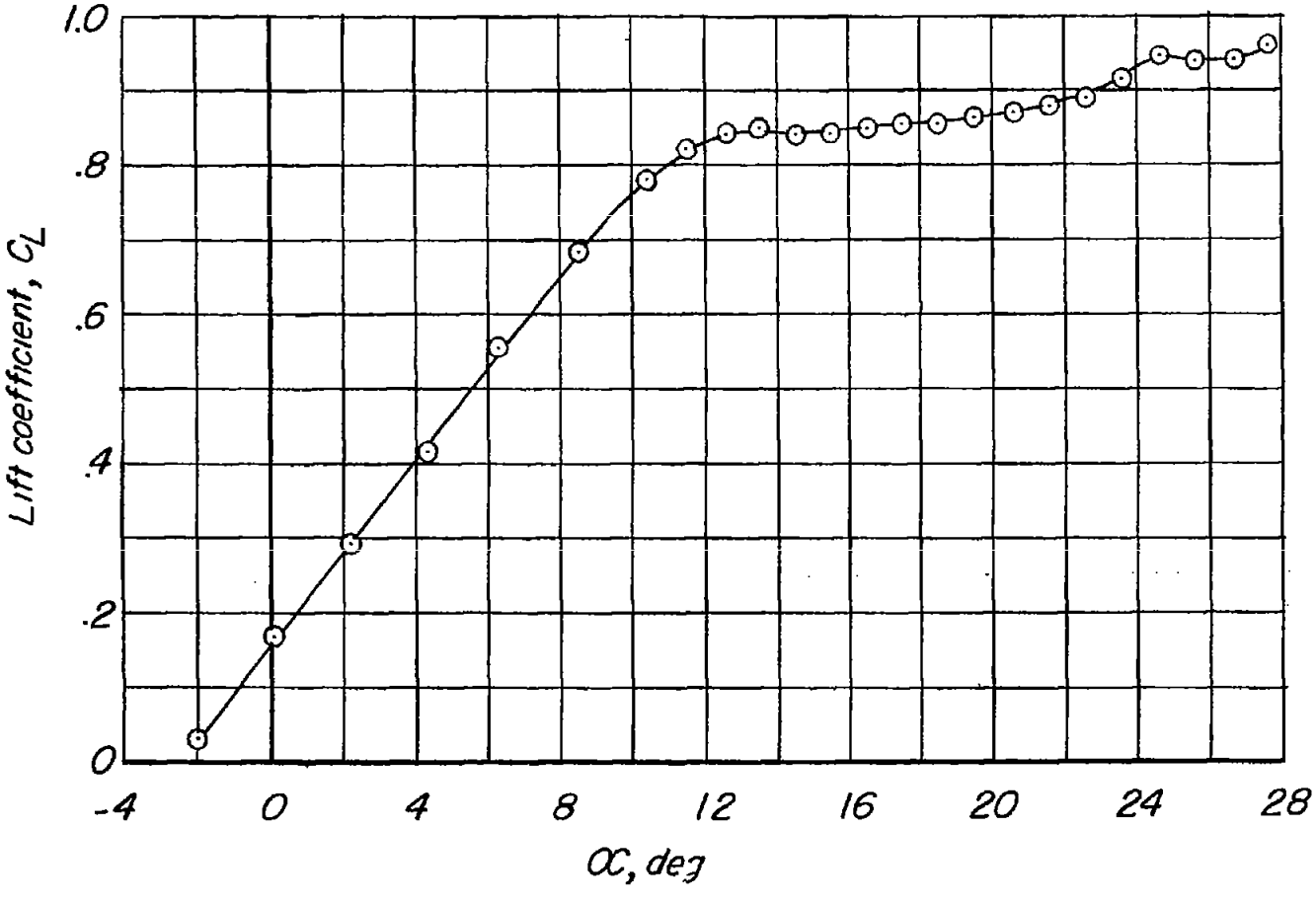

Figure 6.- Variation of C_L with α.

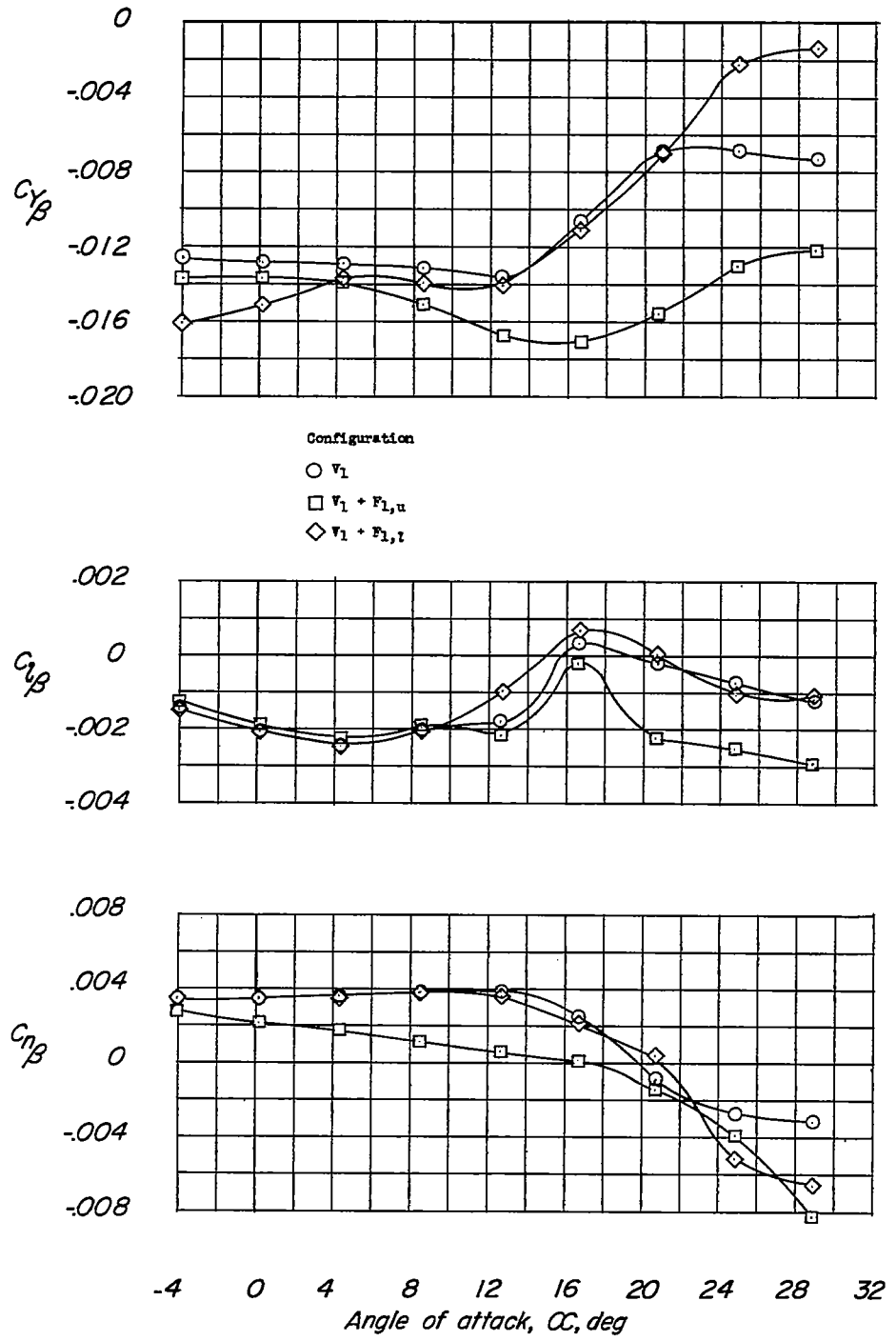

Figure 7.- Static lateral stability derivatives of the model with vertical tail V_1 and several of the vertical fins. Steady-state condition.

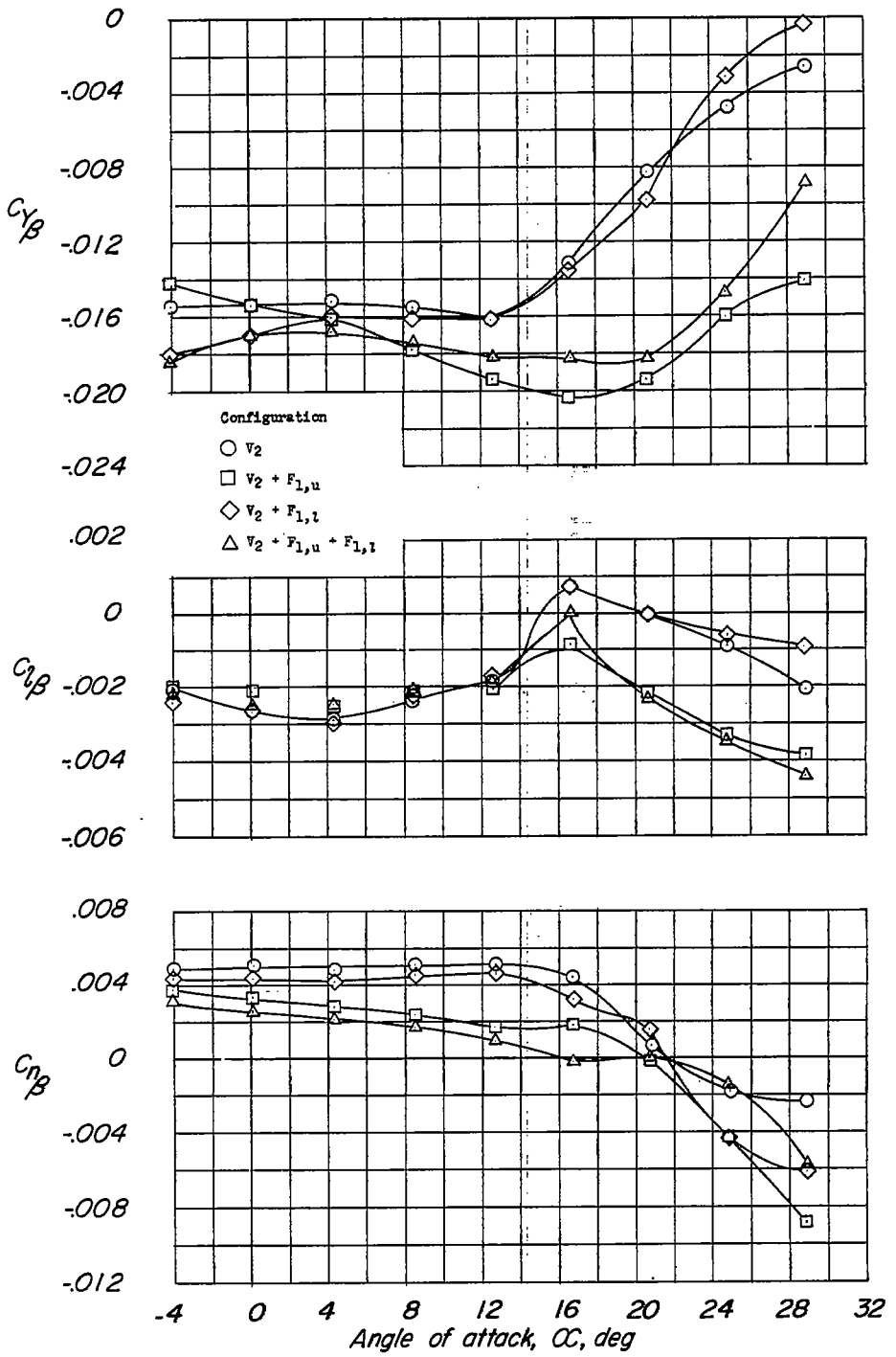

Figure 8.- Static lateral stability derivatives of the model with vertical tail V_2 and several vertical fins. Steady-state condition.

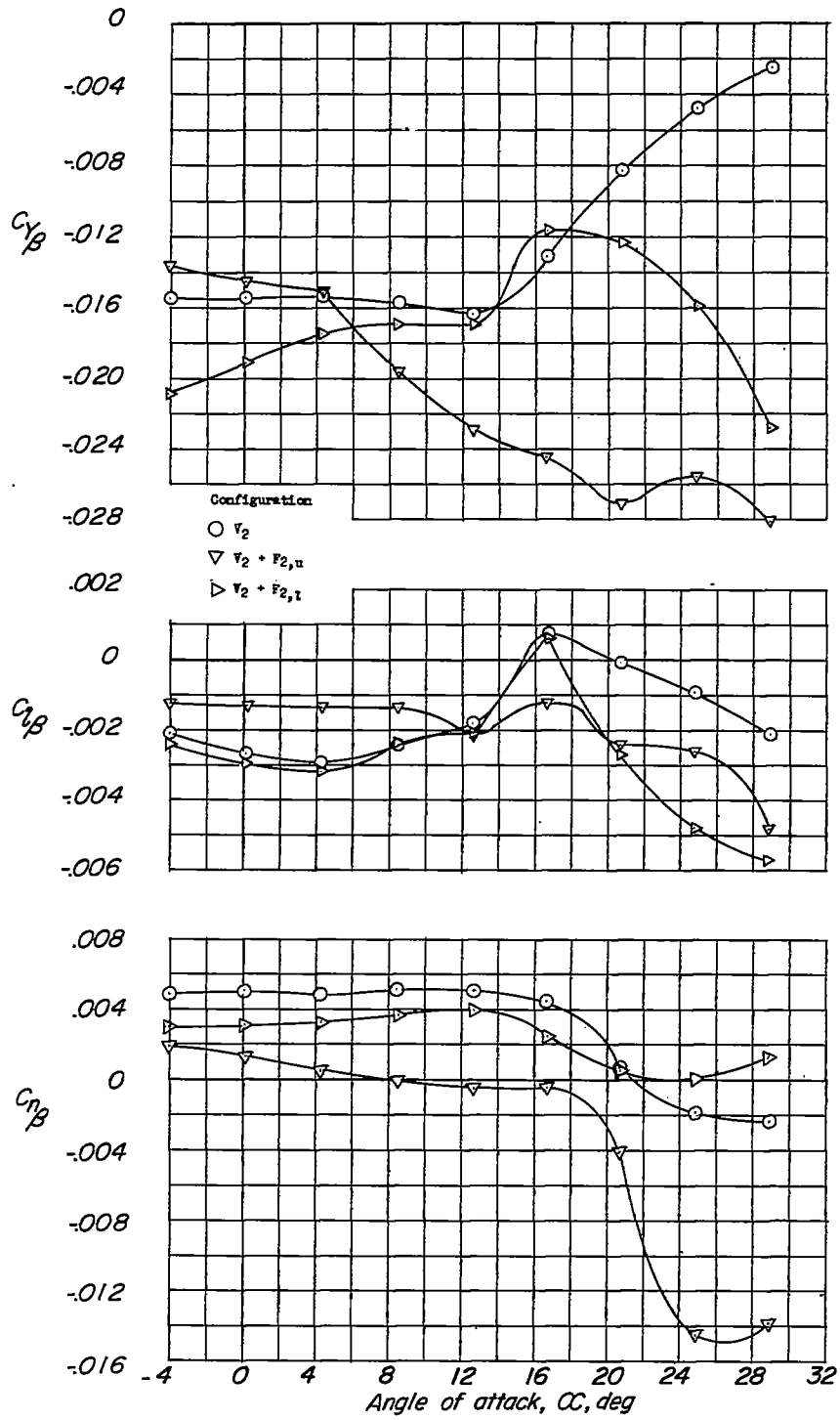

Figure 8.- Concluded.

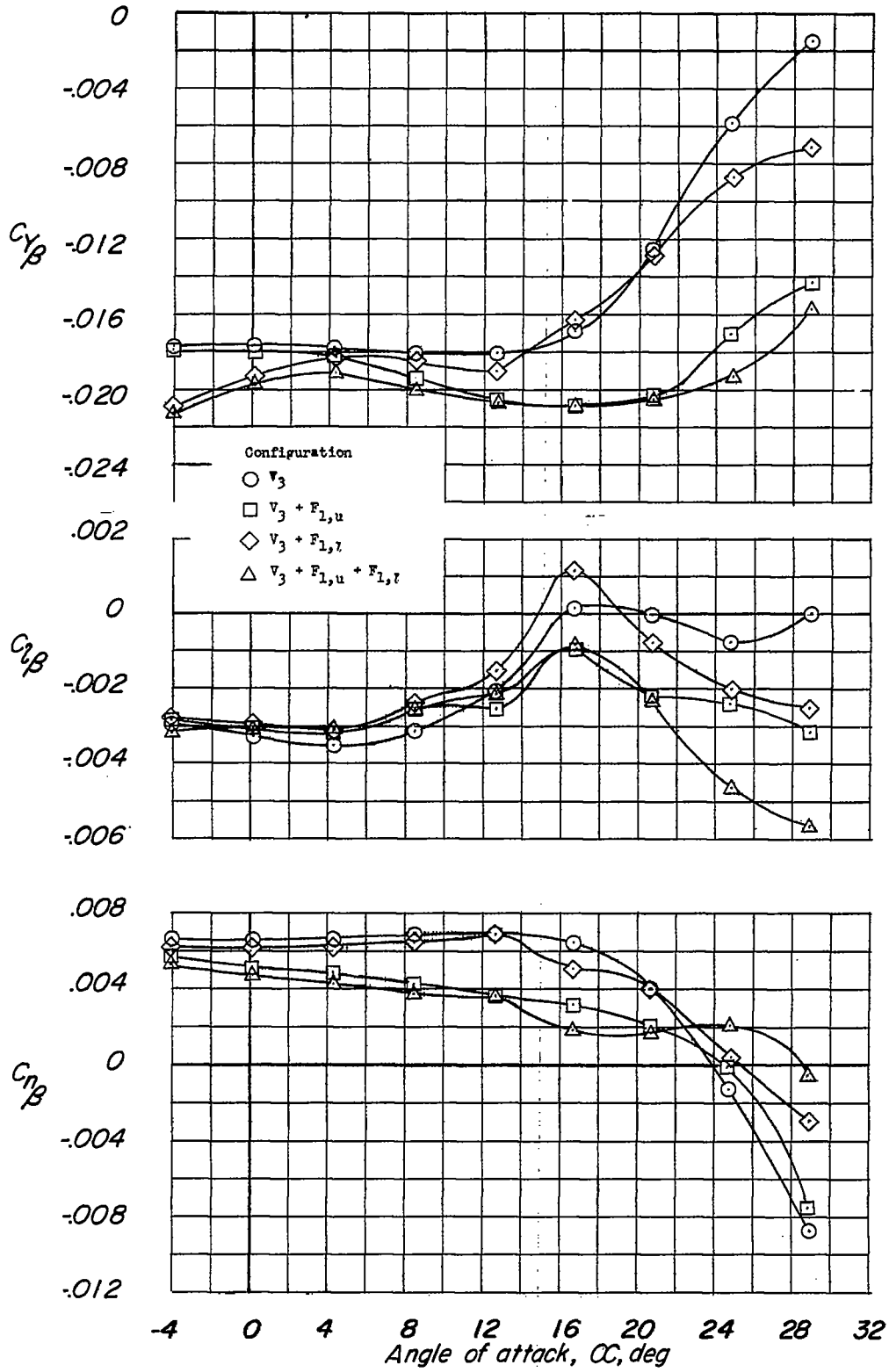

Figure 9.- Static lateral stability derivatives of the model with vertical tail V_3 and several vertical fins. Steady-state condition.

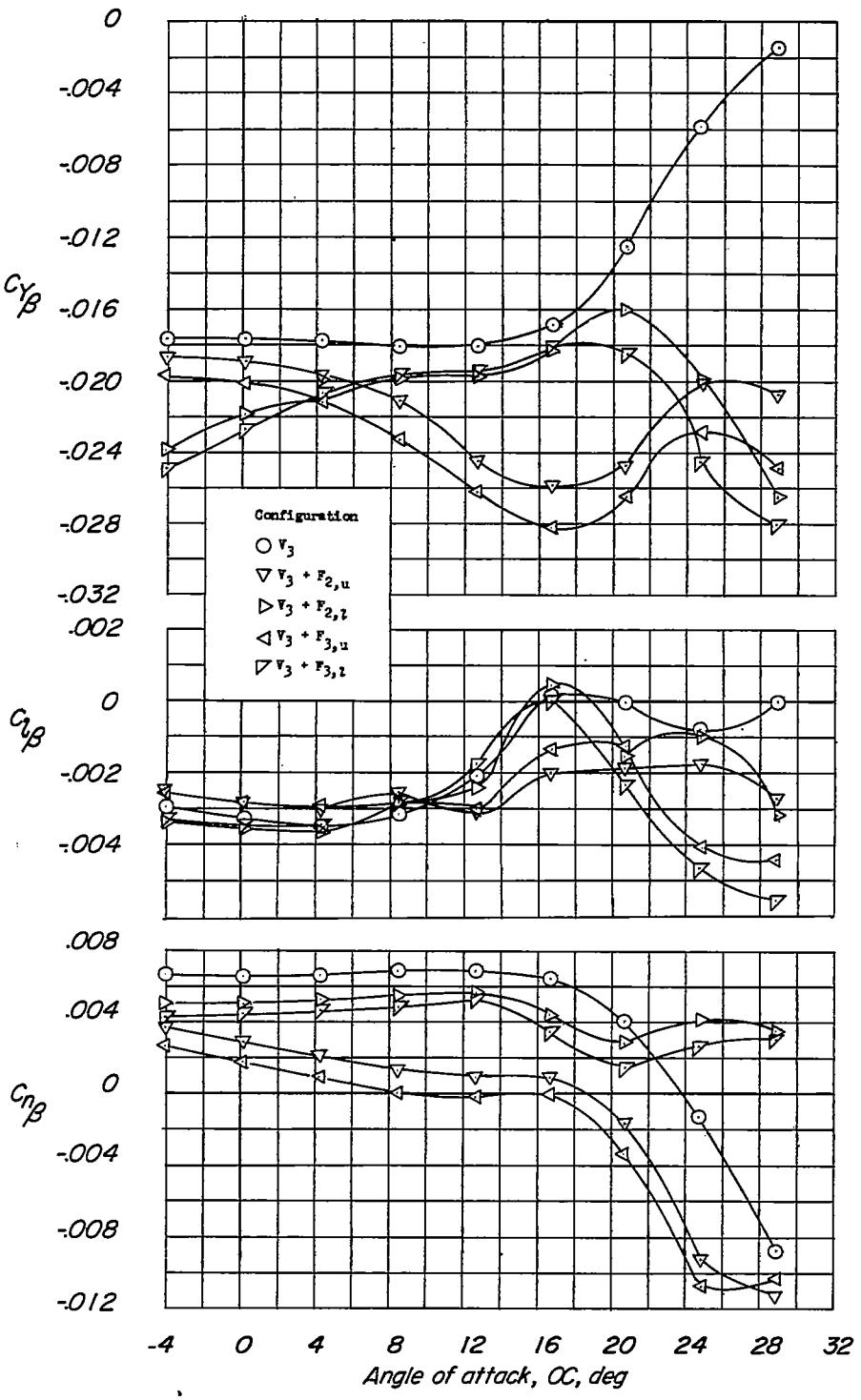

Figure 9.- Continued.

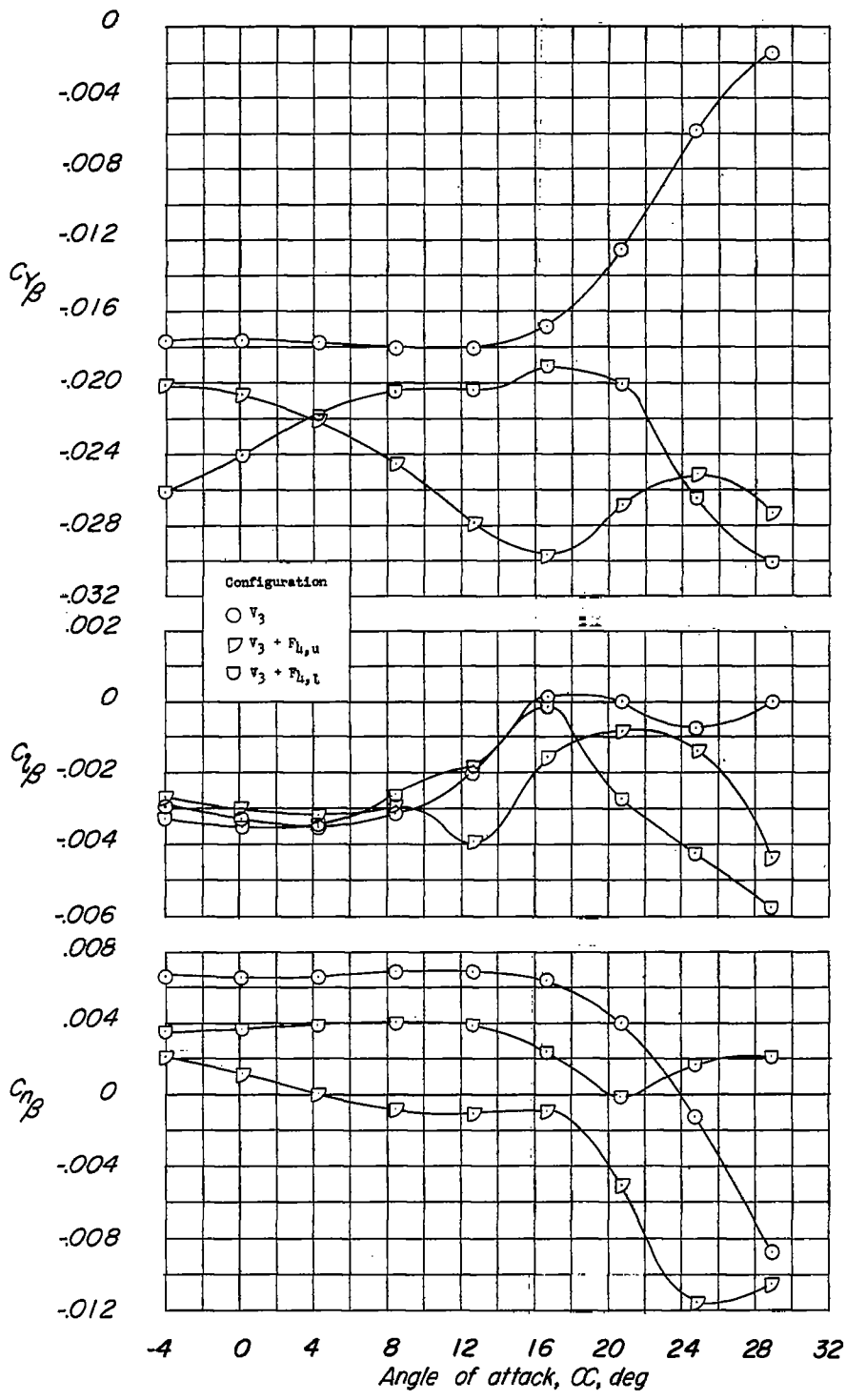

Figure 9.- Concluded.

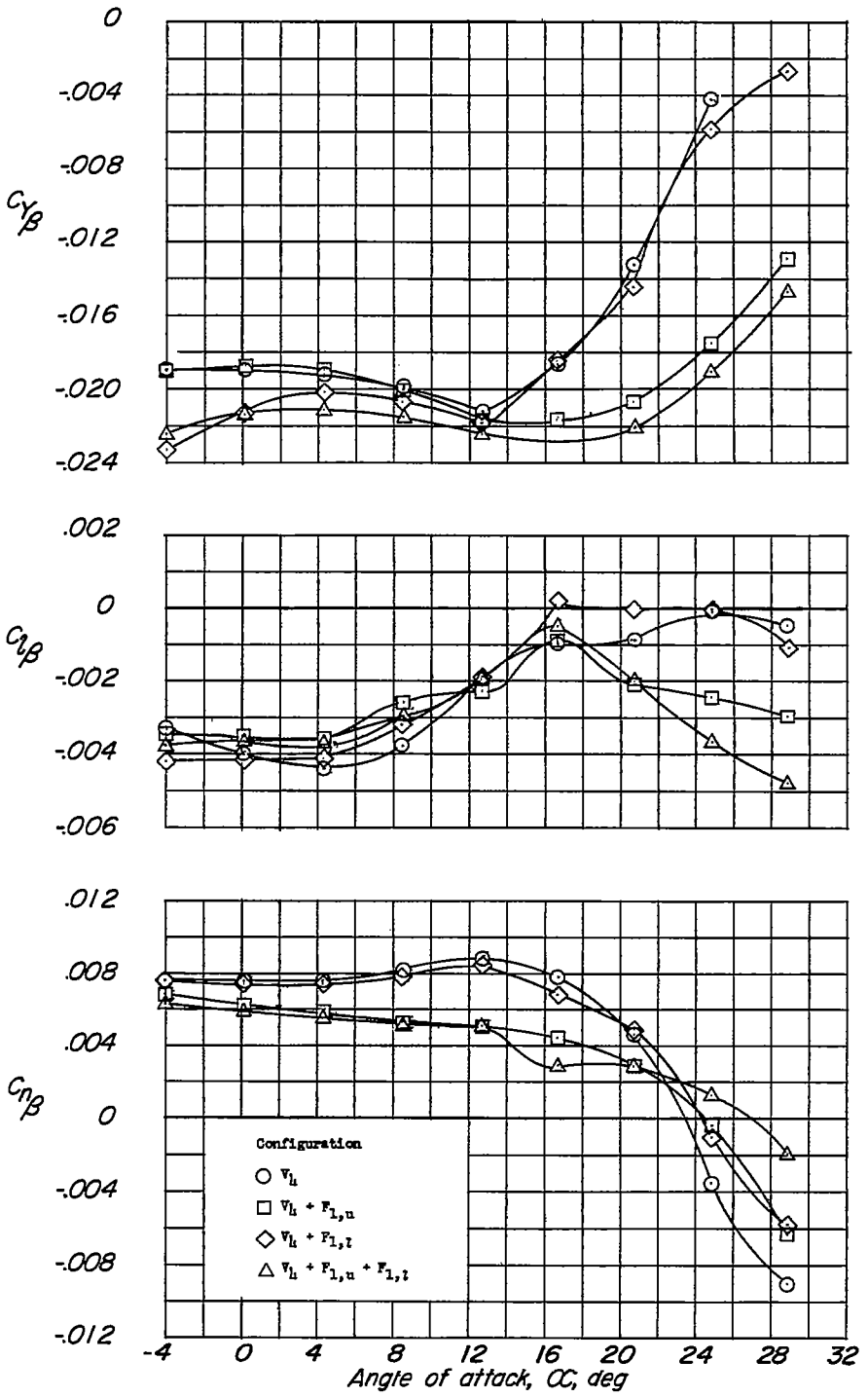

Figure 10.- Static lateral stability derivatives of the model with vertical tail V_4 and several vertical fins. Steady-state condition.

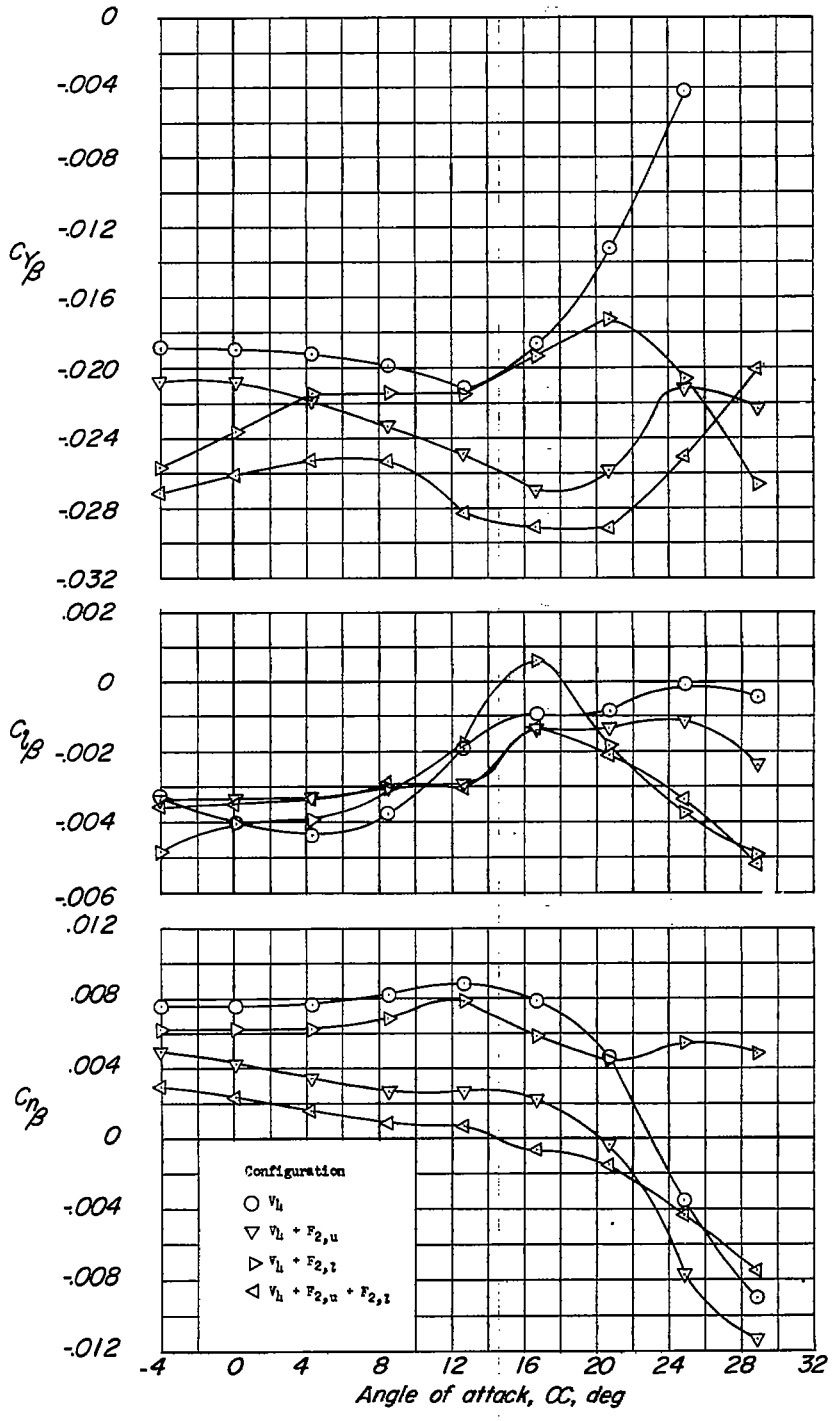

Figure 10.- Continued.

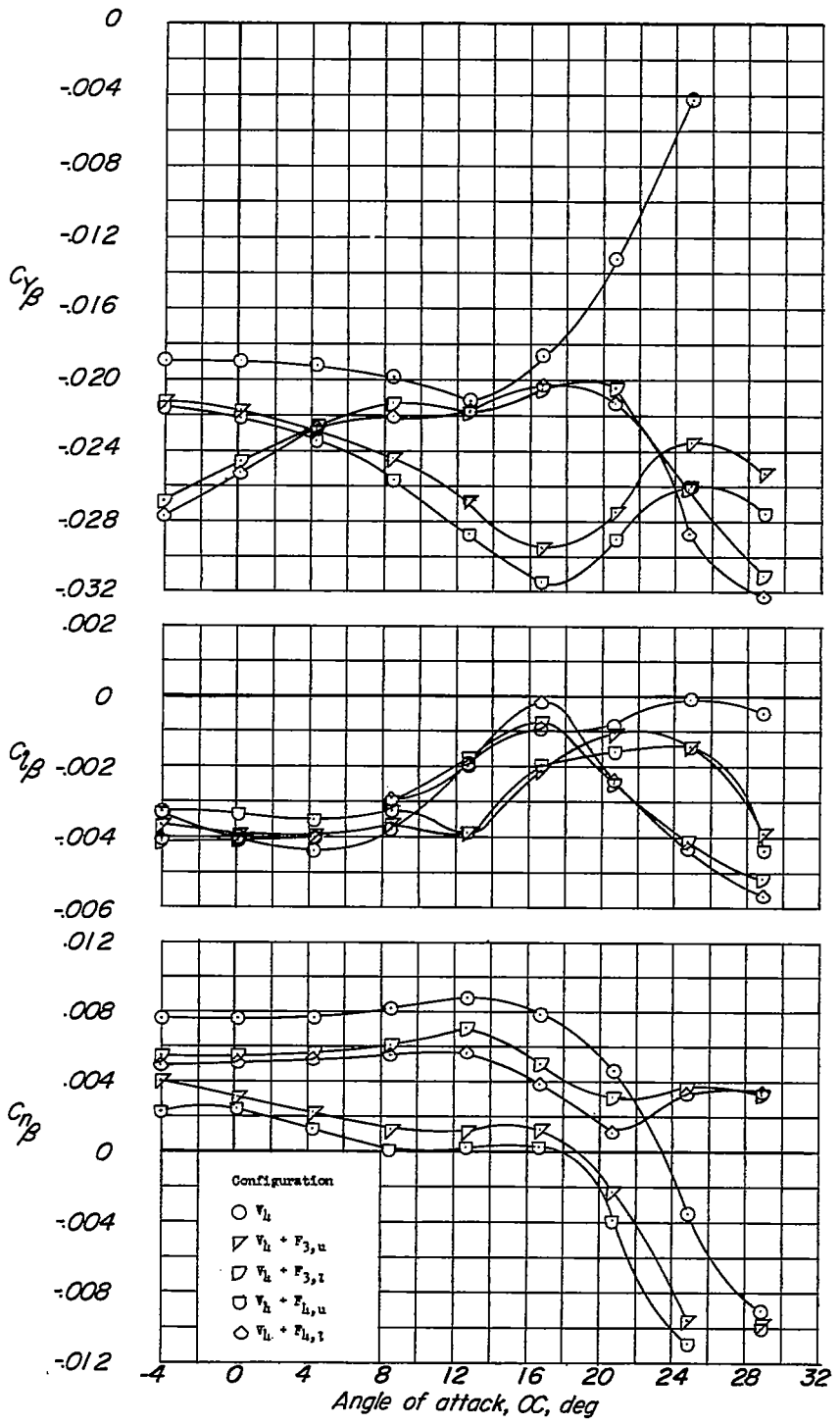

Figure 10.- Concluded.

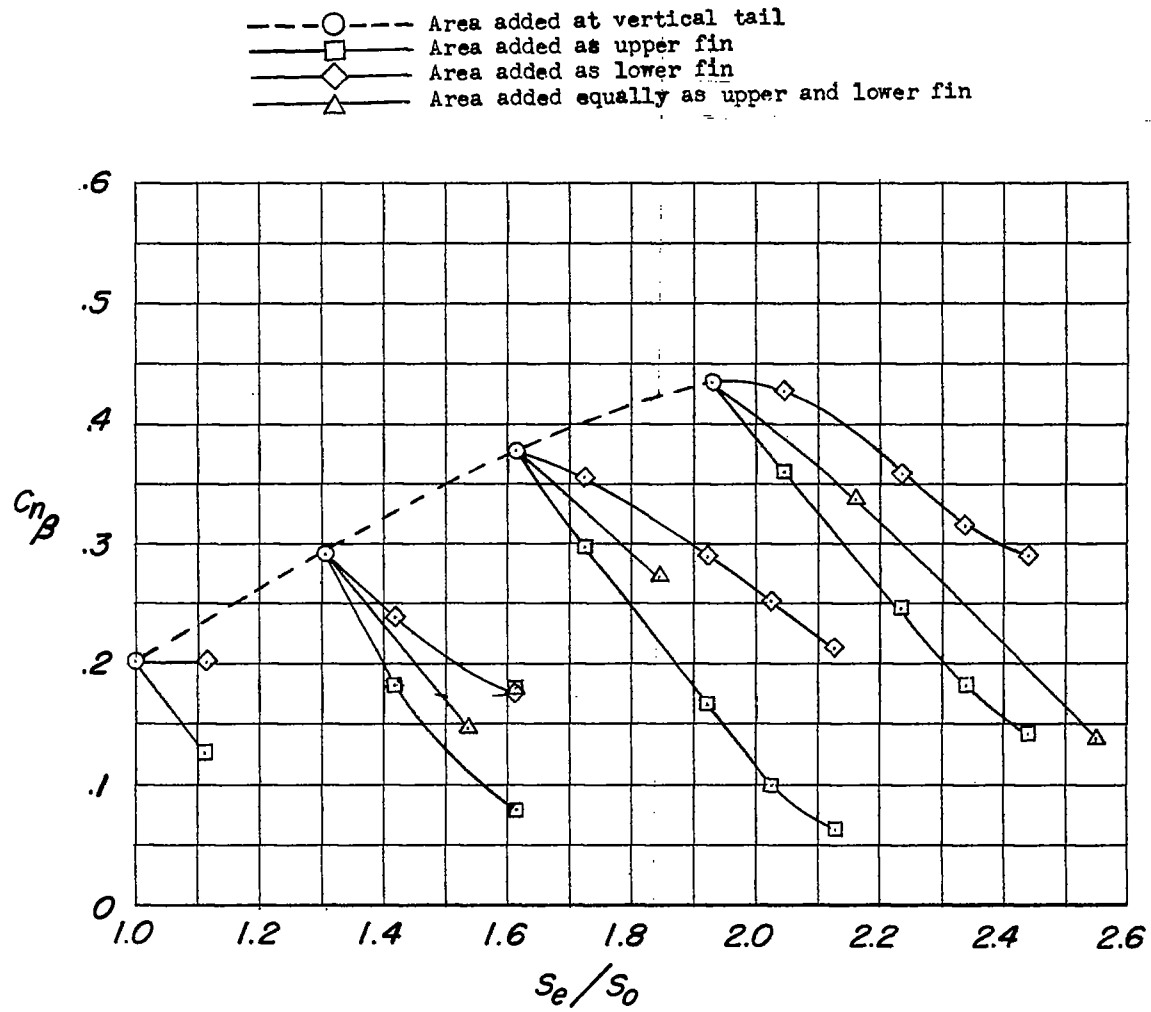

(a) $\alpha = 0^\circ$.

Figure 11.- Variation of C_{n_β} with exposed vertical tail and fin area as measured in steady-state tests.

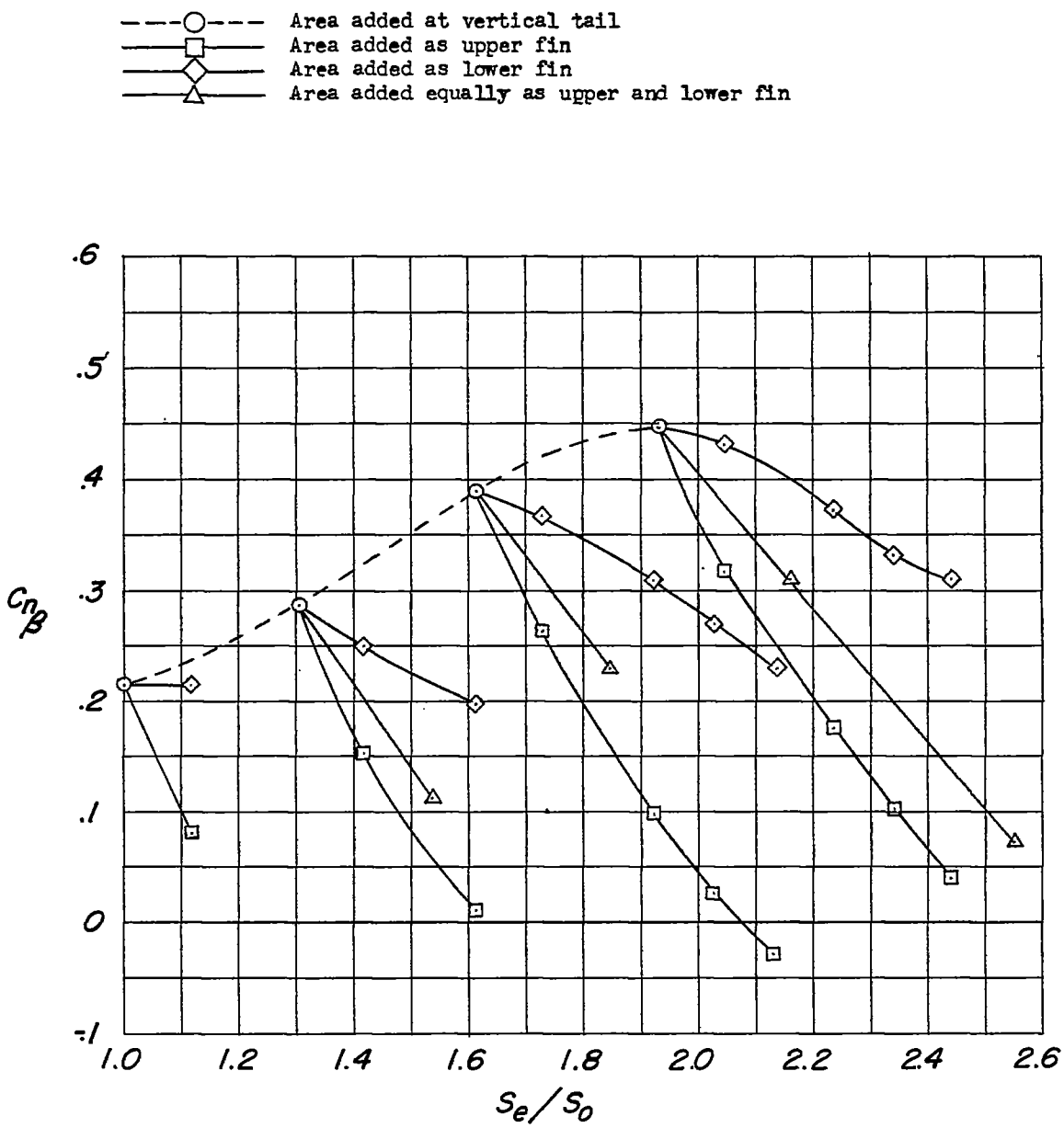

(b) $\alpha = 6^\circ$.

Figure 11.- Continued.

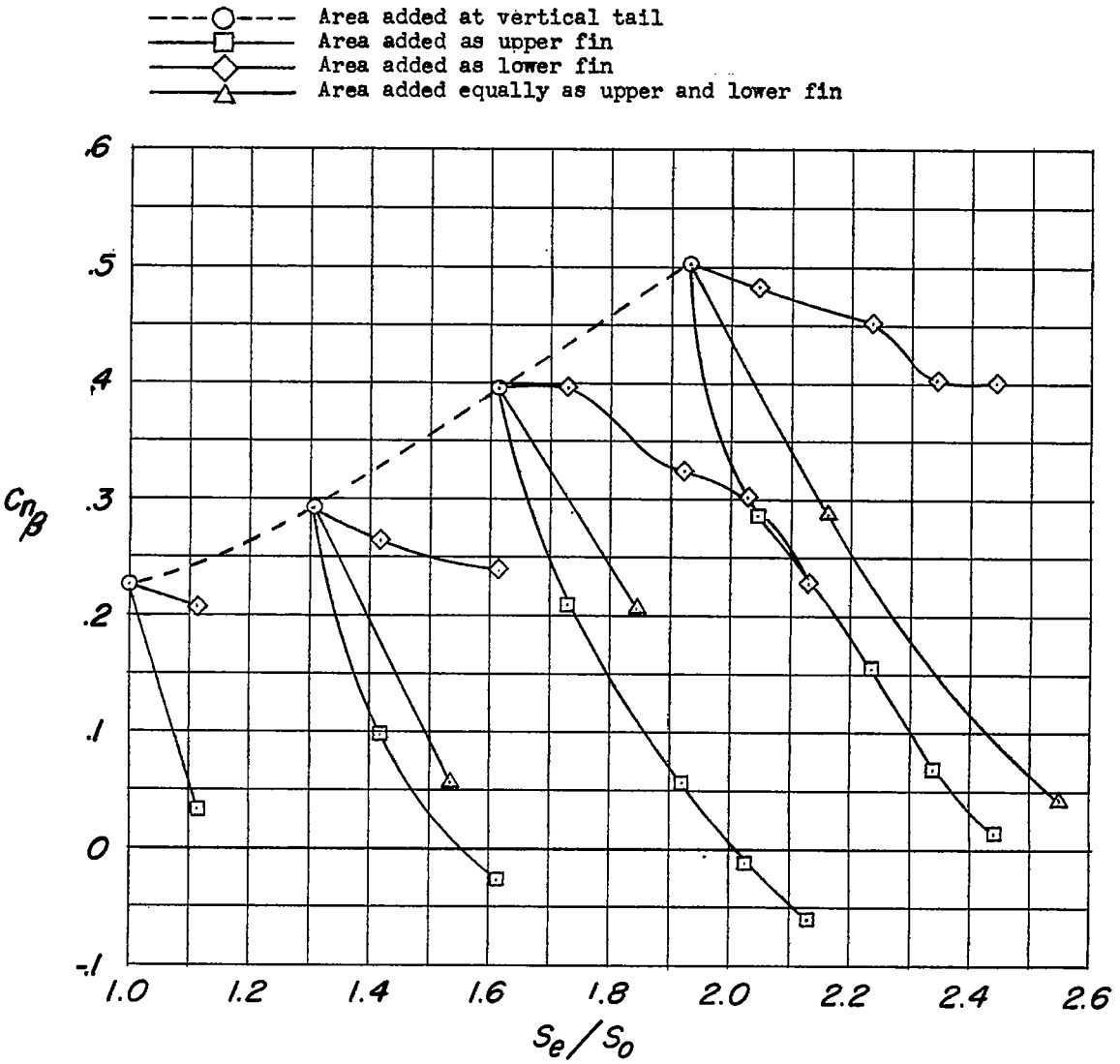

(c) $\alpha = 12^\circ$.

Figure 11.- Concluded.

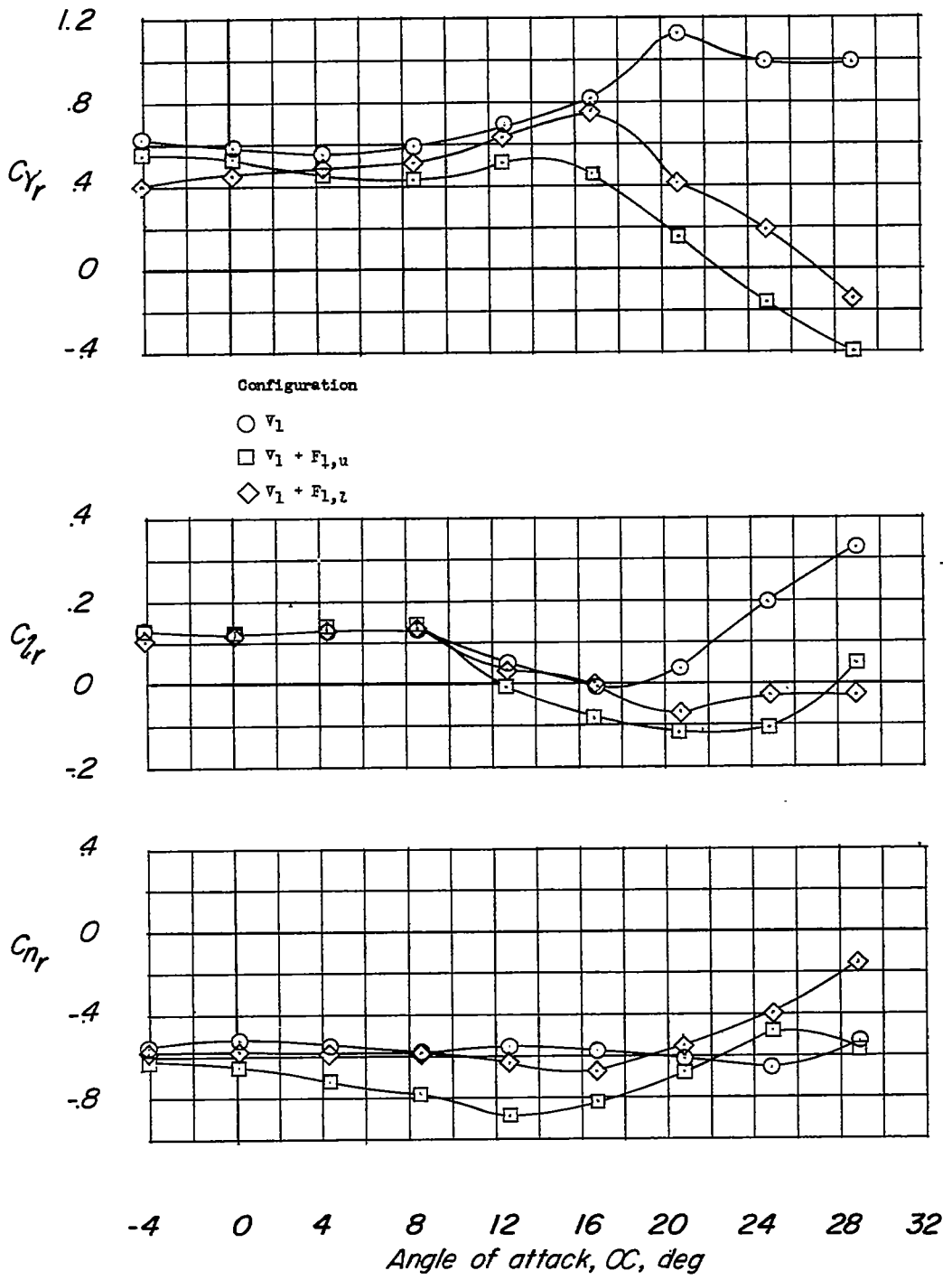

Figure 12.- Steady-state yawing derivatives of the model with vertical tail V_1 and several vertical fins.

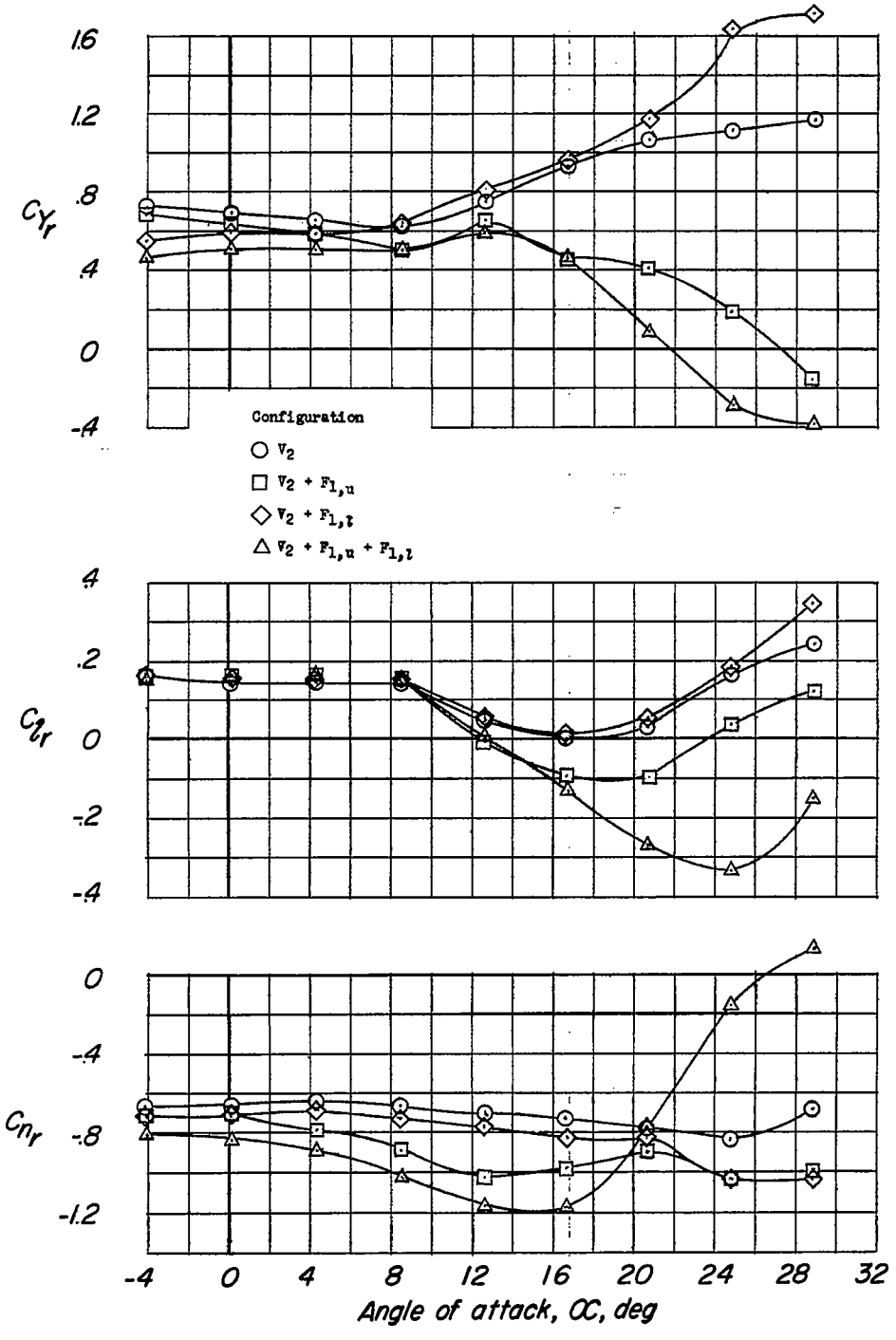

Figure 13.- Steady-state yawing derivatives of the model with vertical tail V_2 and several vertical fins.

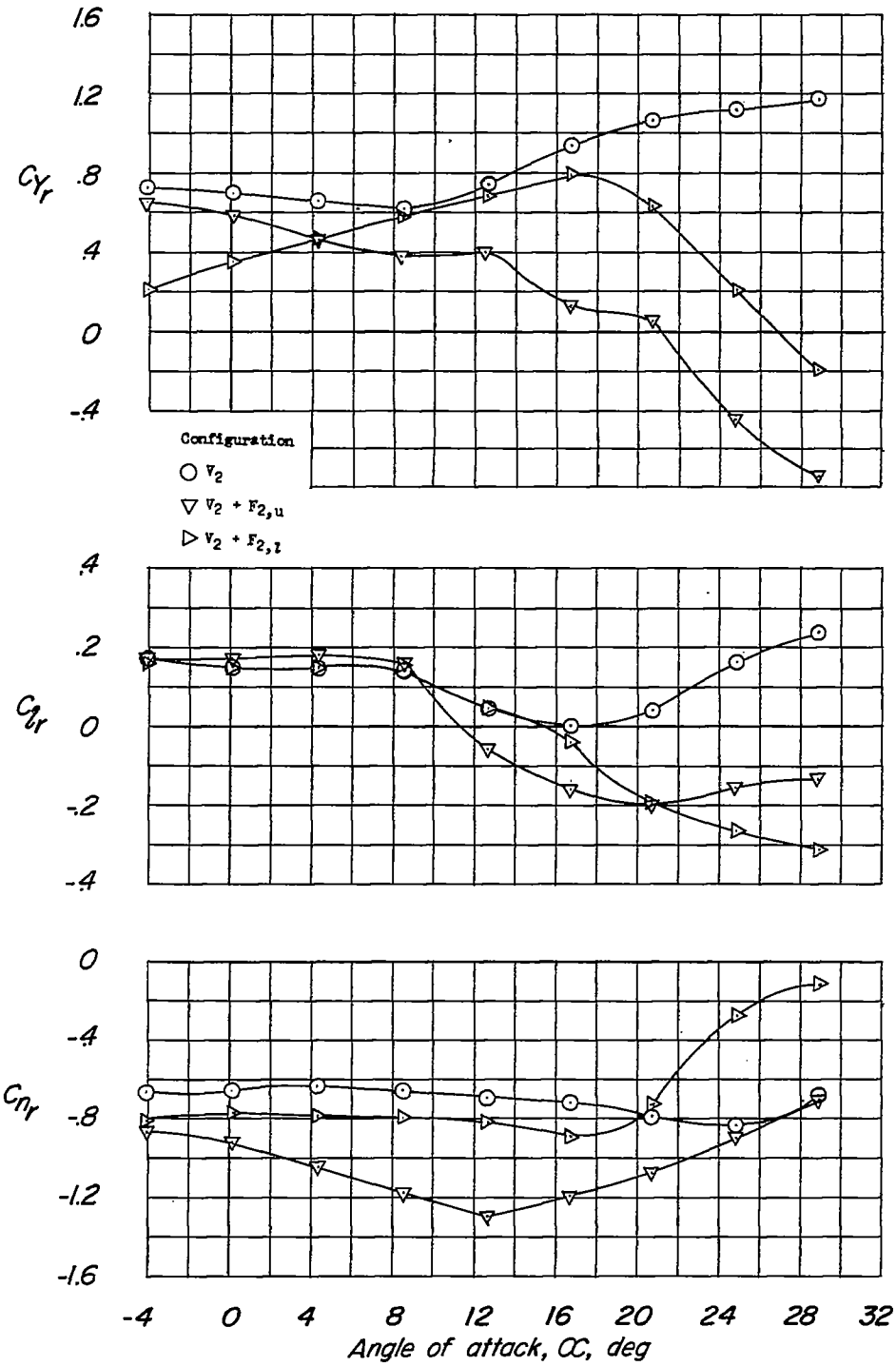

Figure 13.- Concluded.

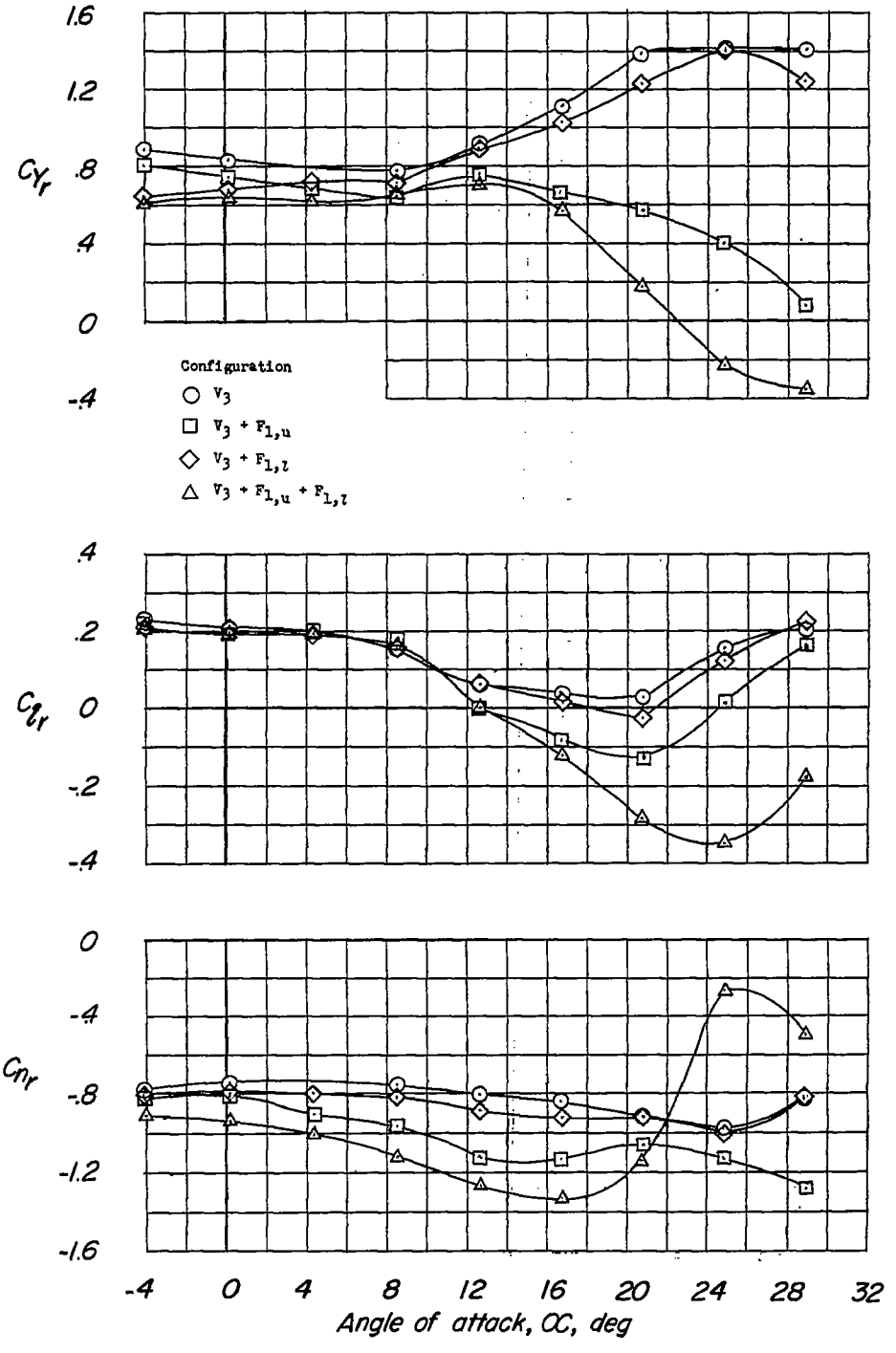

Figure 14.- Steady-state yawing derivatives of the model with vertical tail V_3 and several vertical fins.

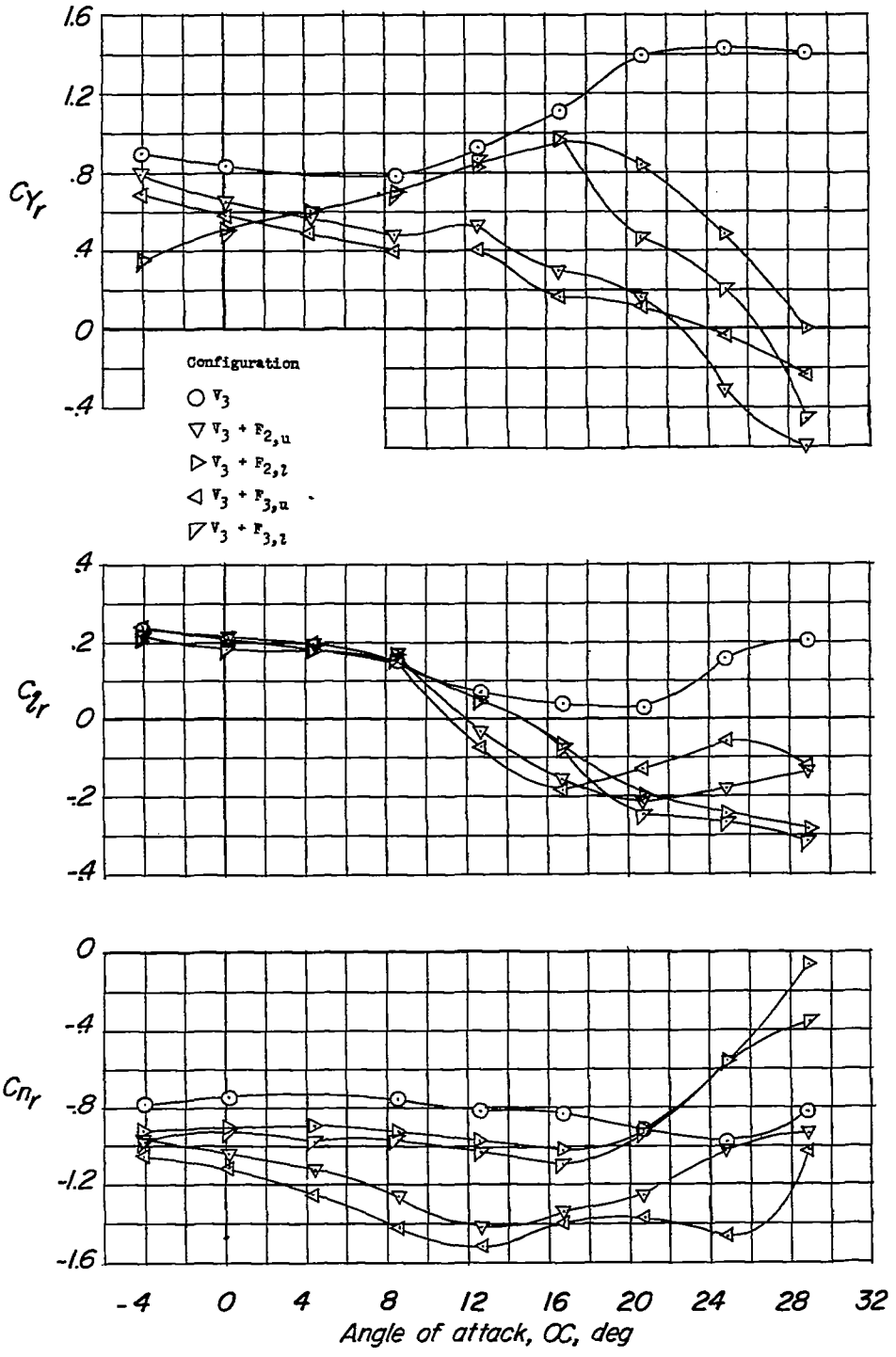

Figure 14.- Continued.

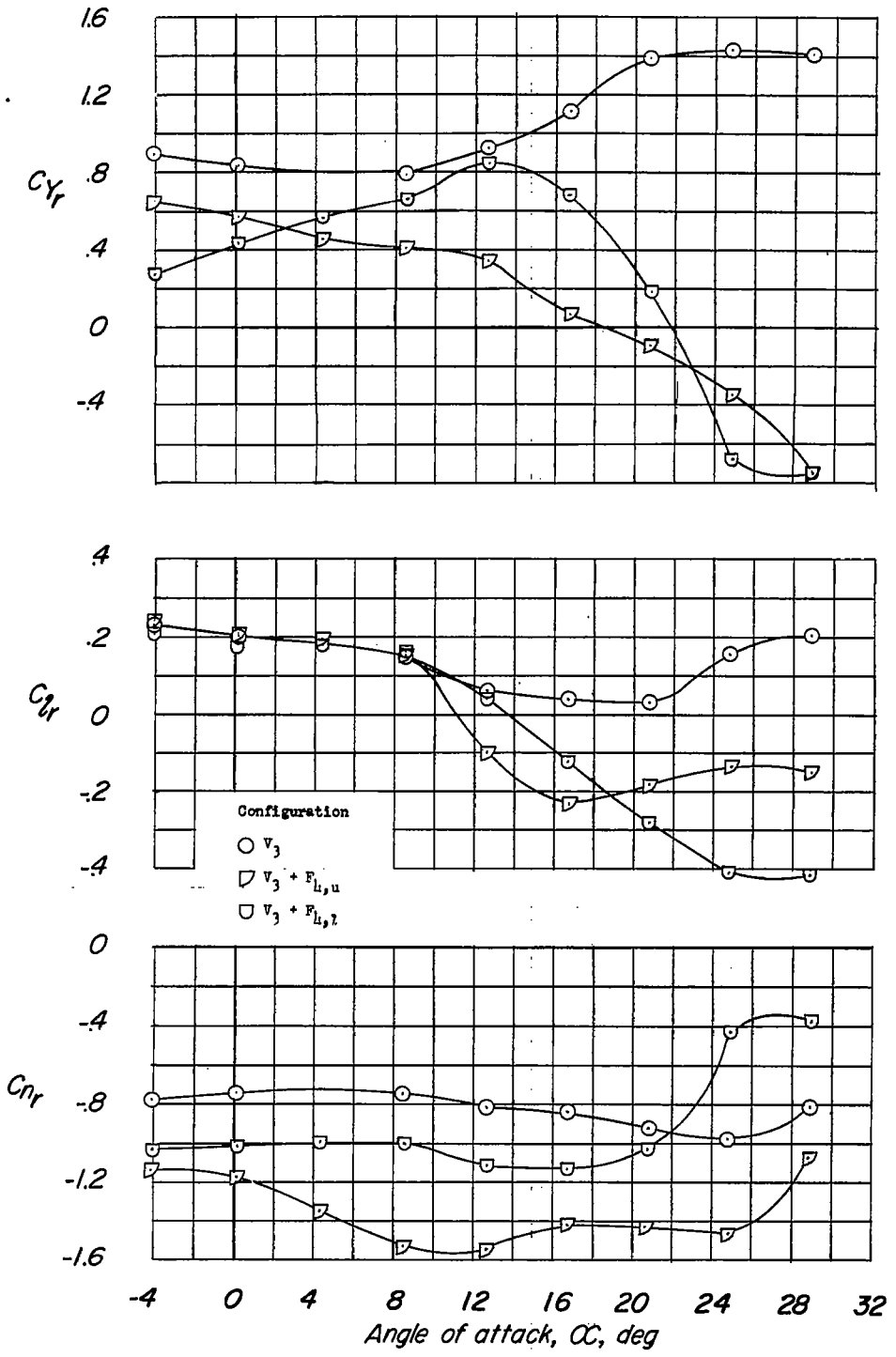

Figure 14.- Concluded.

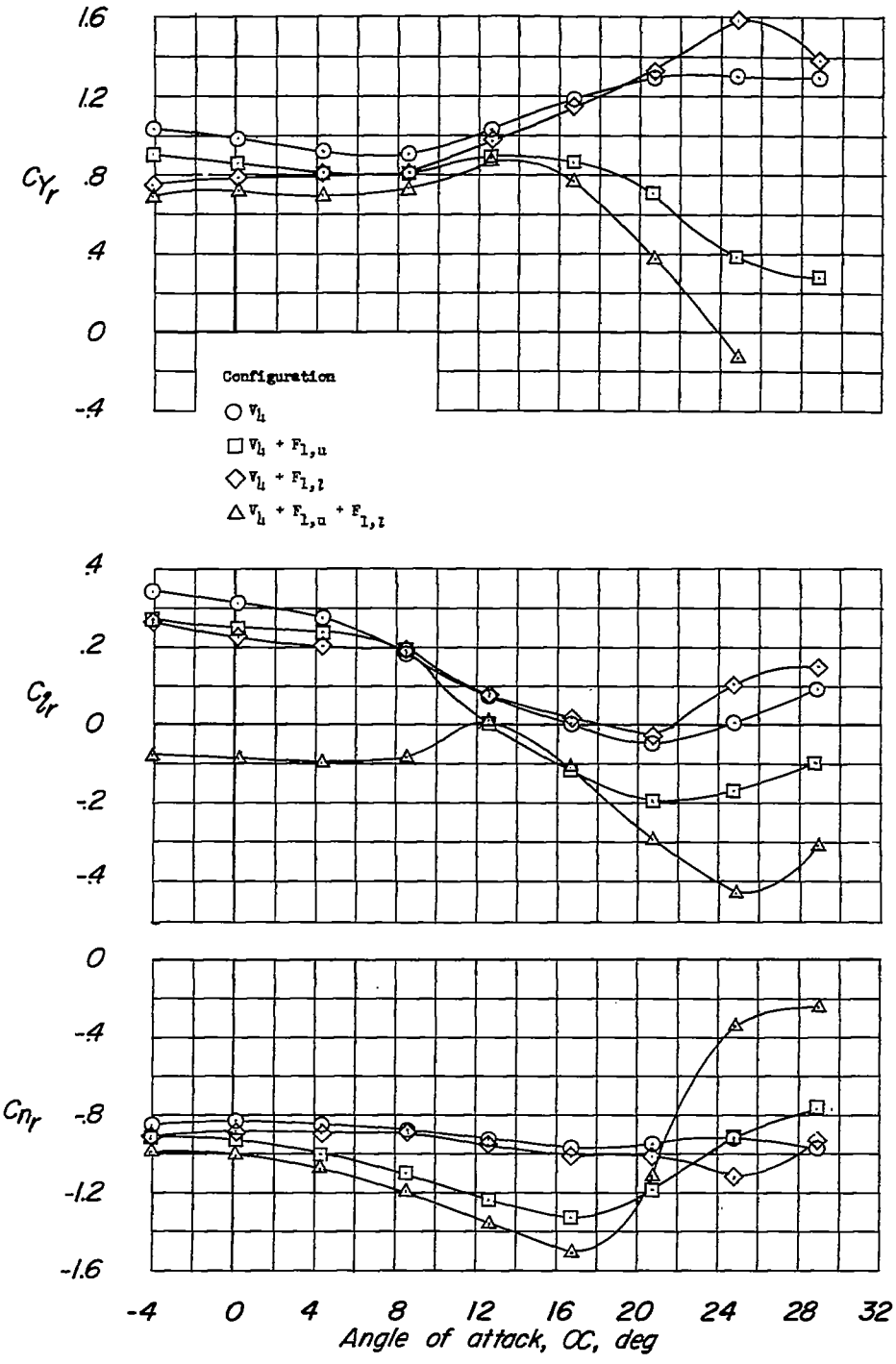

Figure 15.- Steady-state yawing derivatives of the model with vertical tail V_4 and several vertical fins.

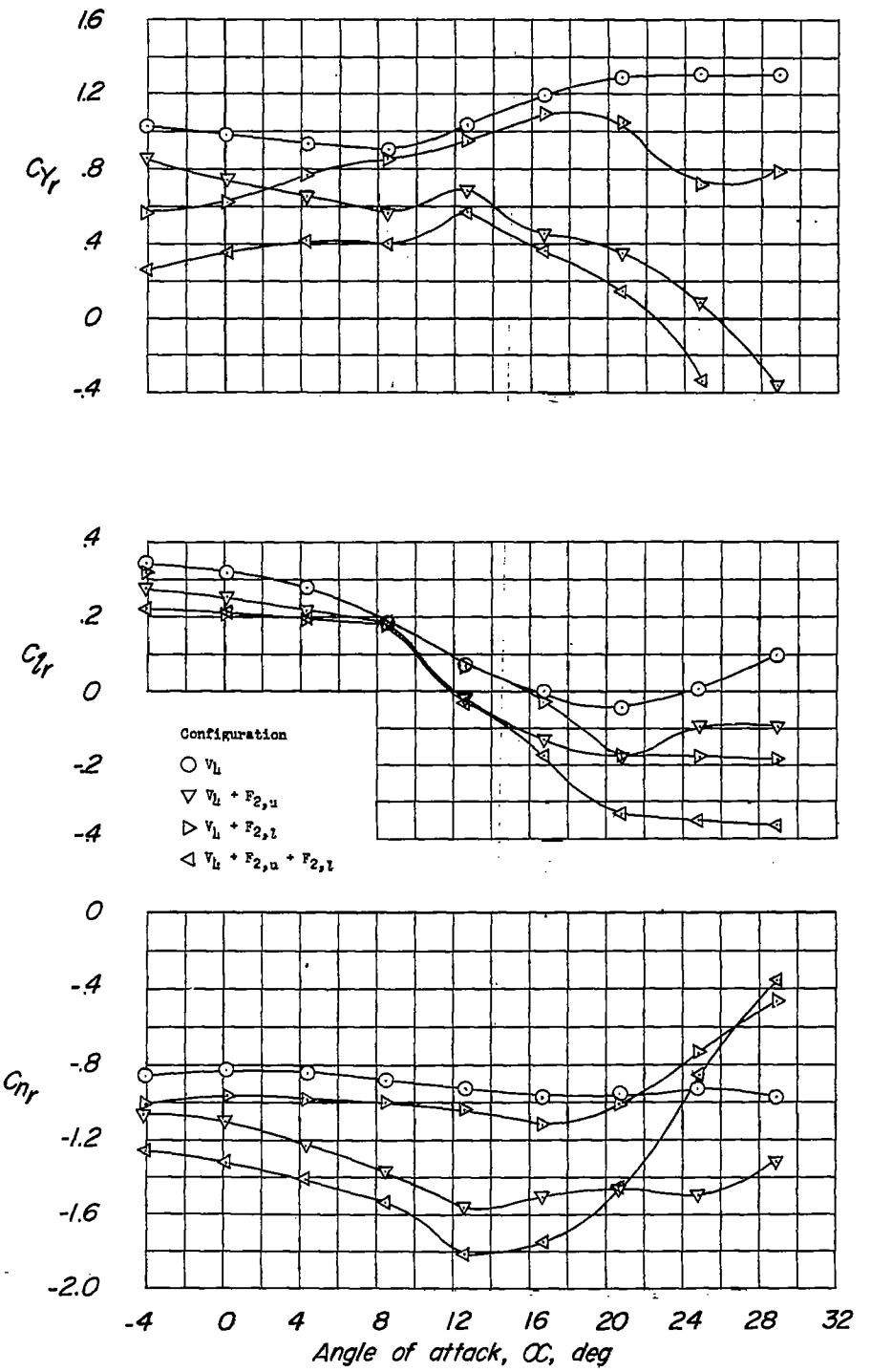

Figure 15.- Continued.

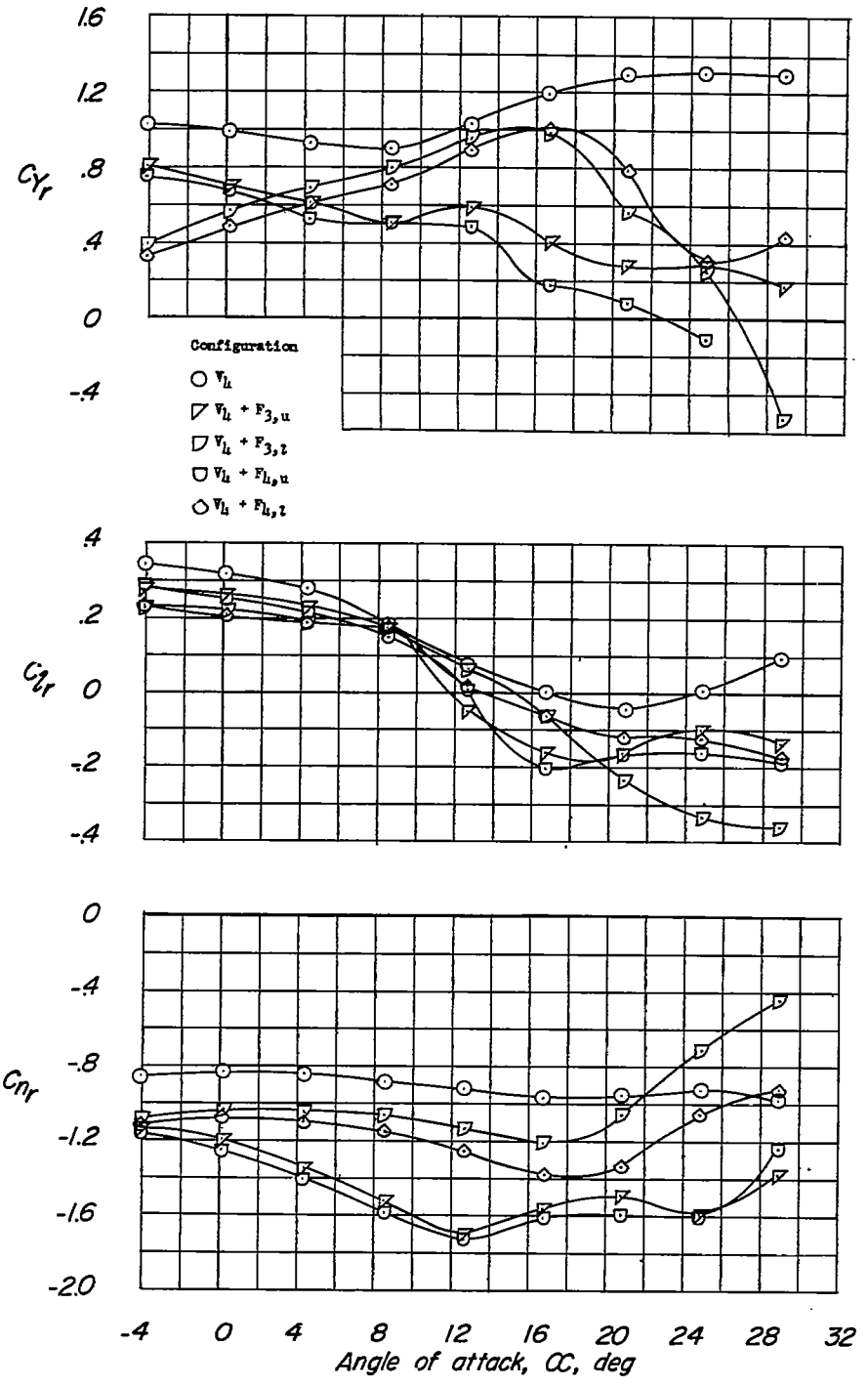

Figure 15.- Concluded.

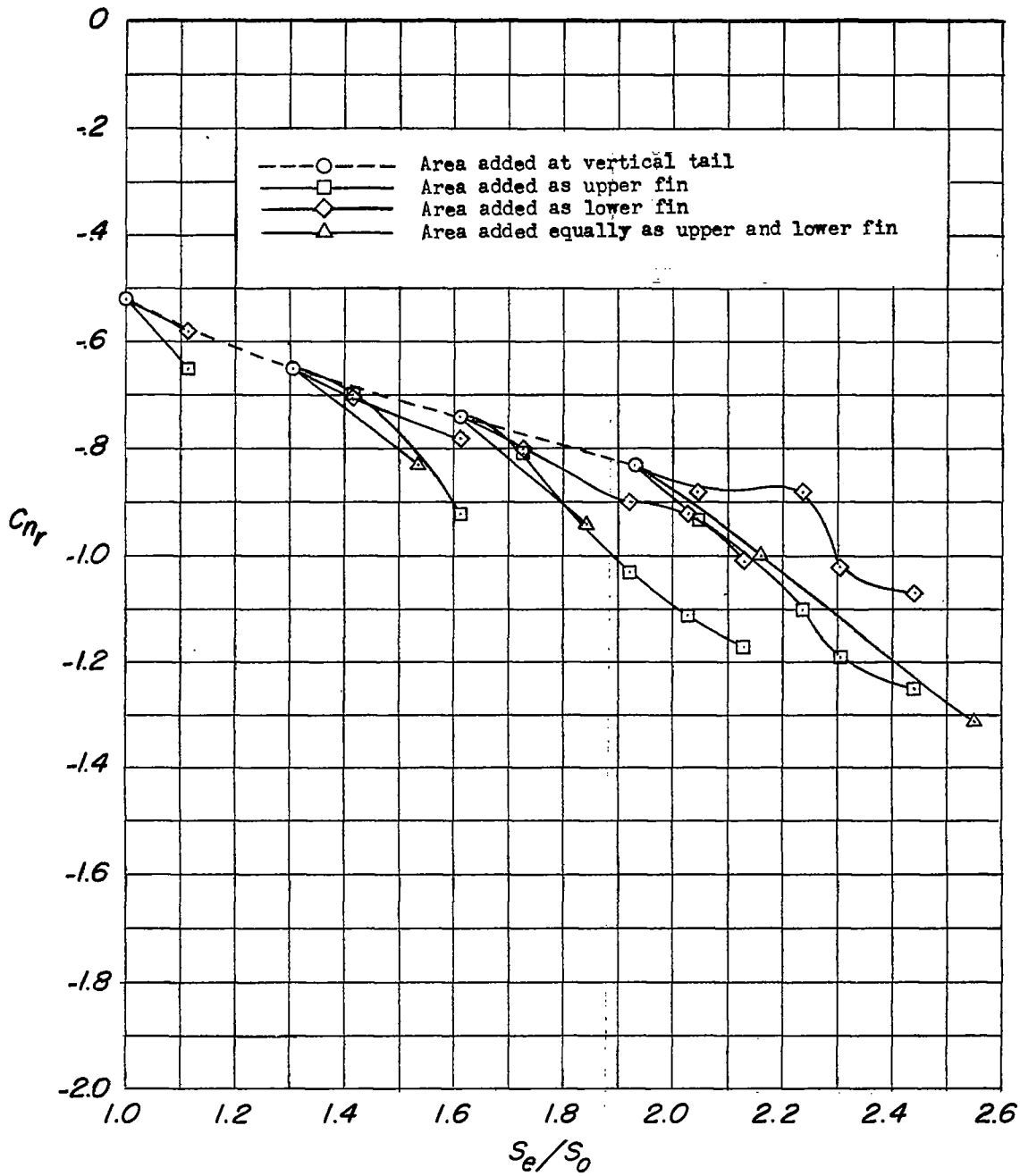

(a) $\alpha = 0^\circ$.

Figure 16.- Variation of C_{n_r} with exposed vertical tail and fin area as measured in steady-state tests.

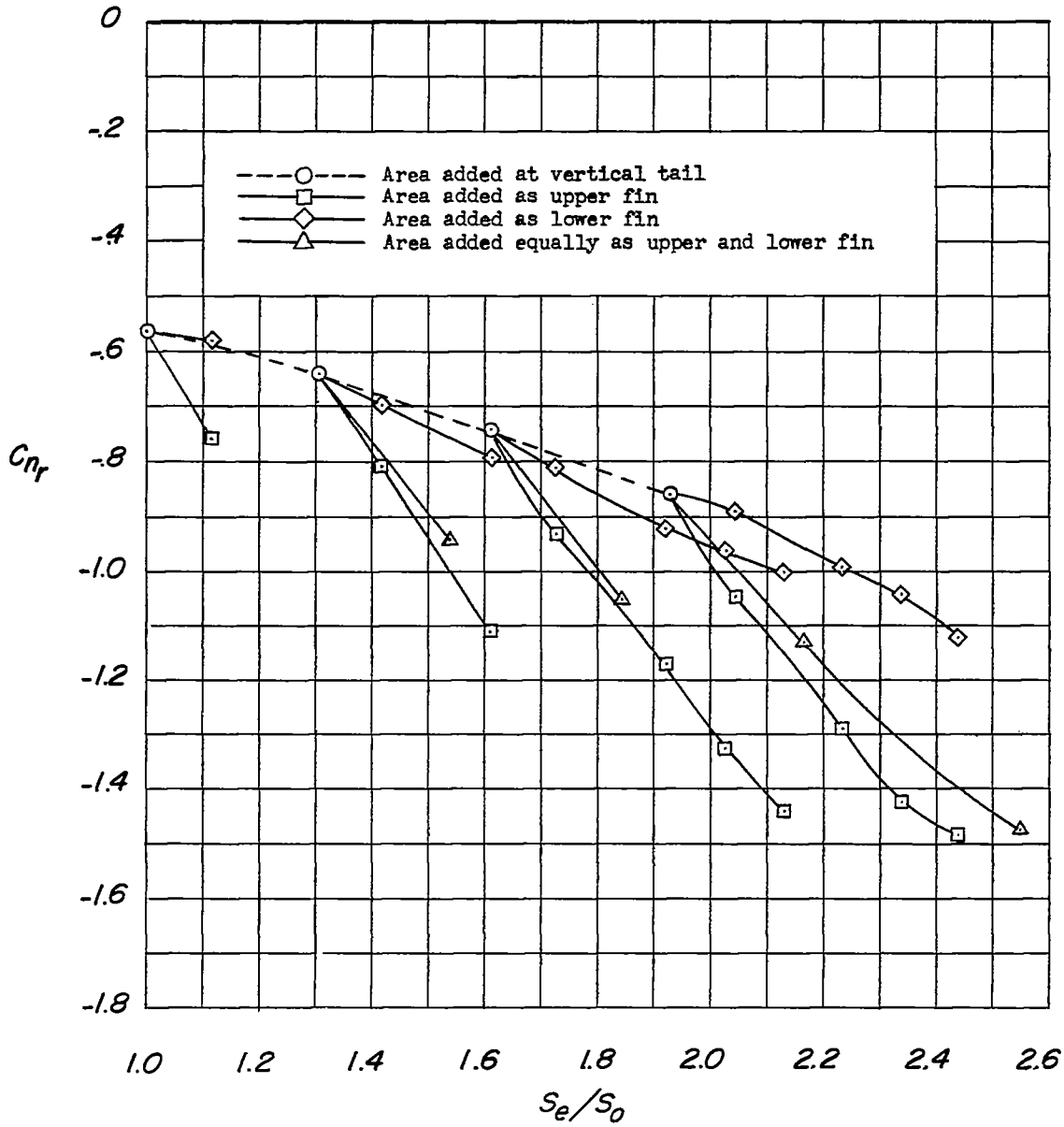

(b) $\alpha = 6.4^\circ$.

Figure 16.- Continued.

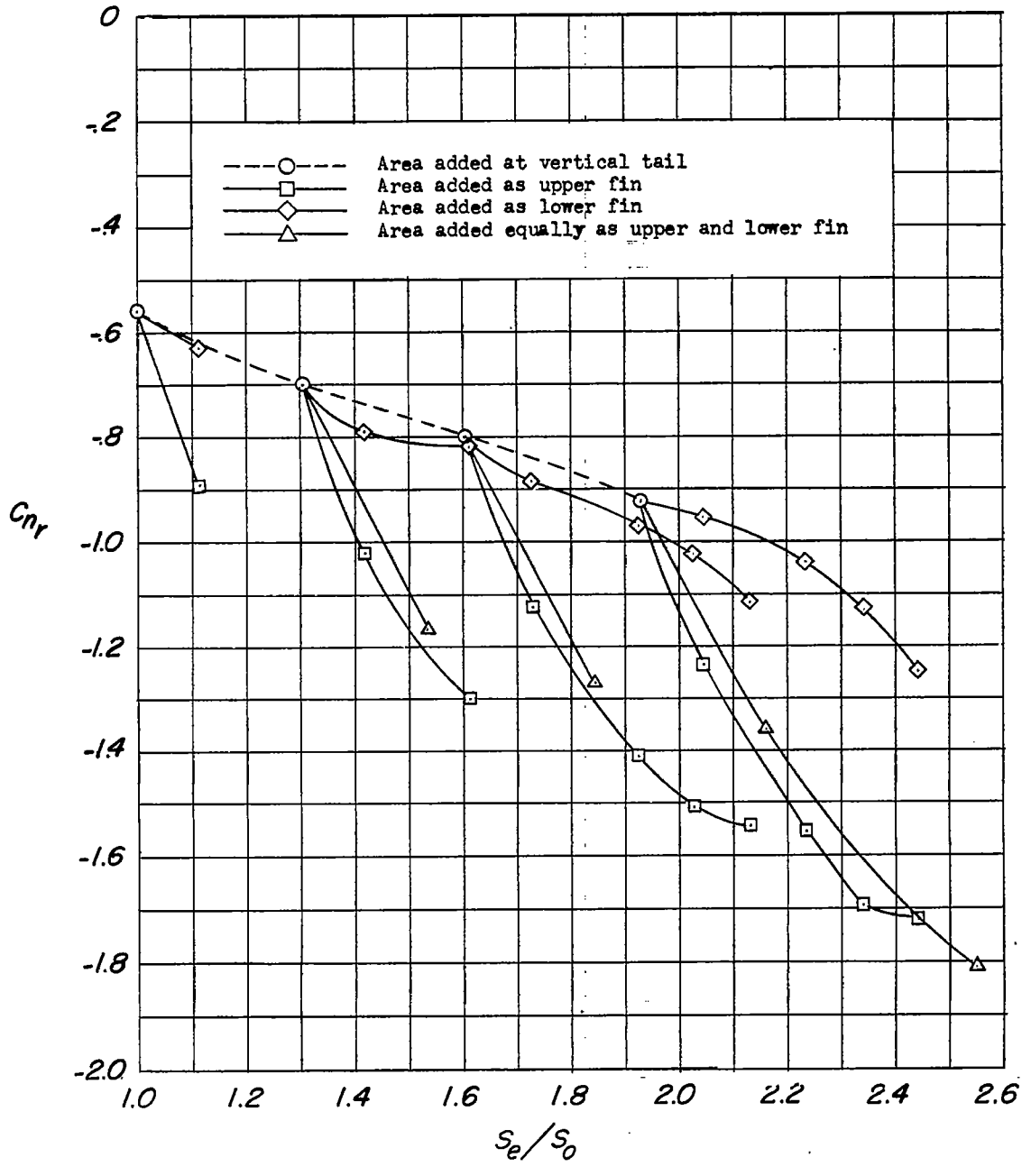

(c) $\alpha = 12.6^{\circ}$.

Figure 16.- Concluded.

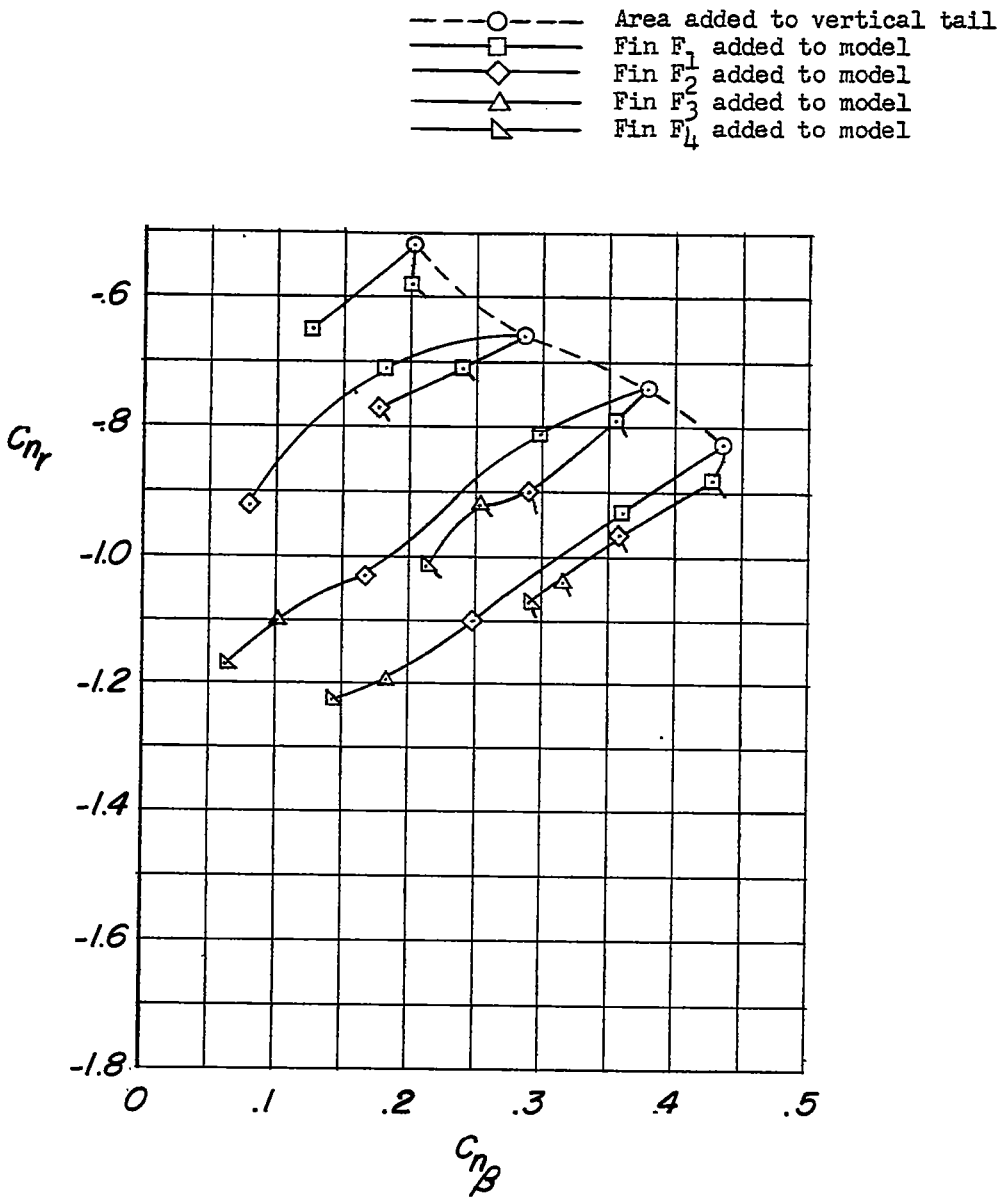

(a) $\alpha = 0^\circ$.

Figure 17.- Values of C_{n_r} and C_{n_β} for the various model configurations. Unflagged symbols indicate upper fin; flagged symbols indicate lower fin.

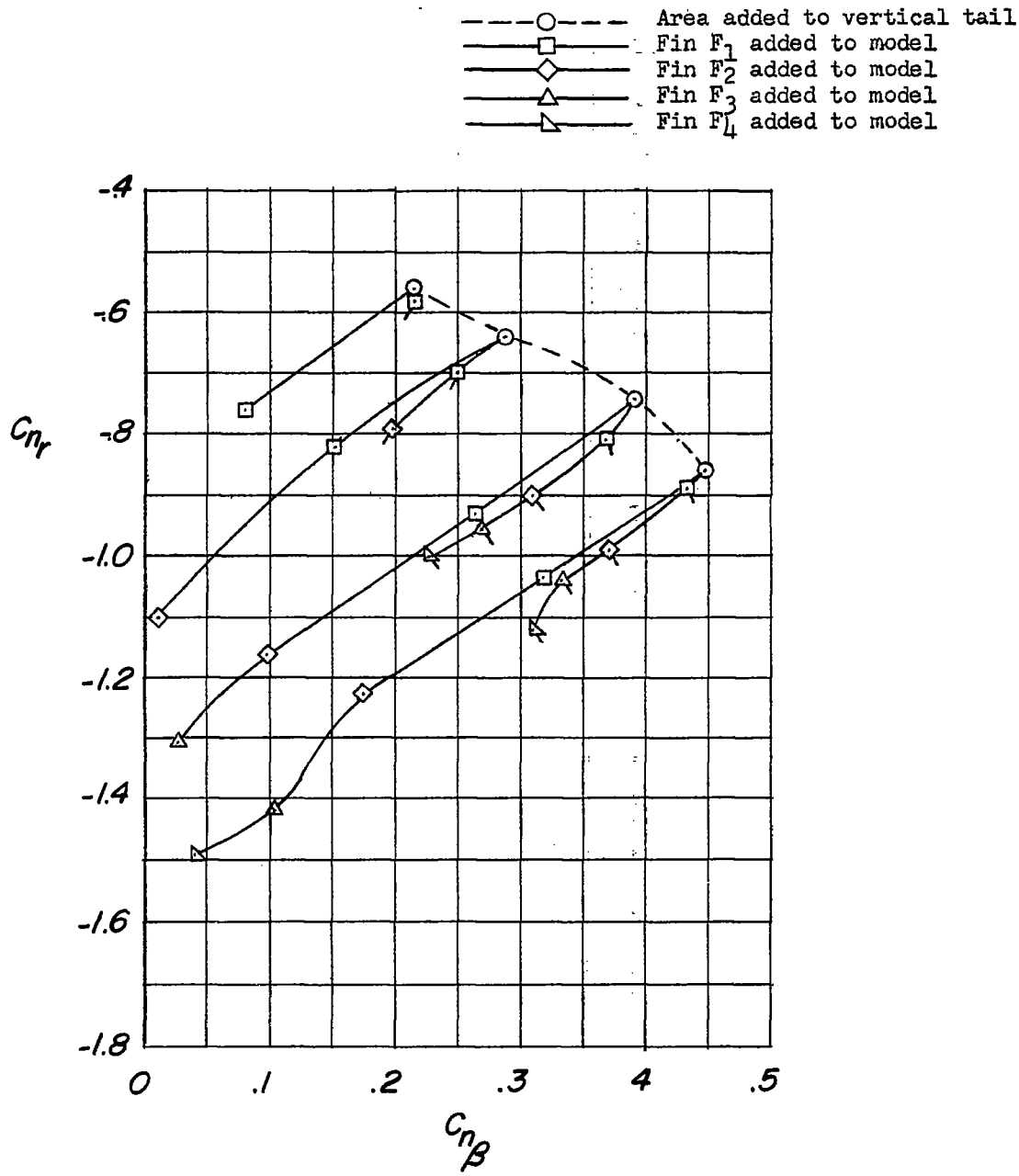

(b) $\alpha = 6.4^\circ$.

Figure 17.- Continued.

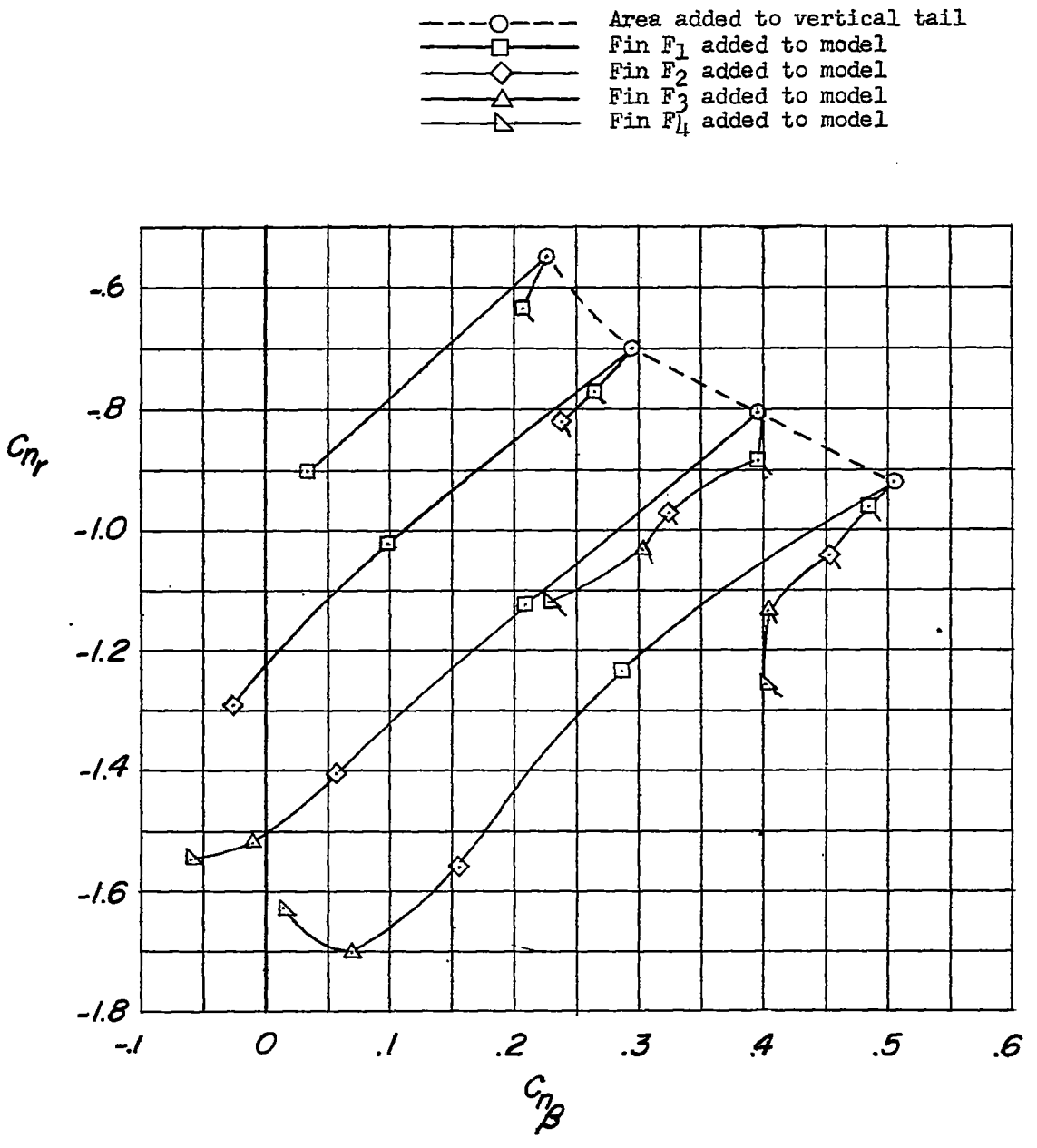

(c) $\alpha = 12.6^\circ$.

Figure 17.- Concluded.

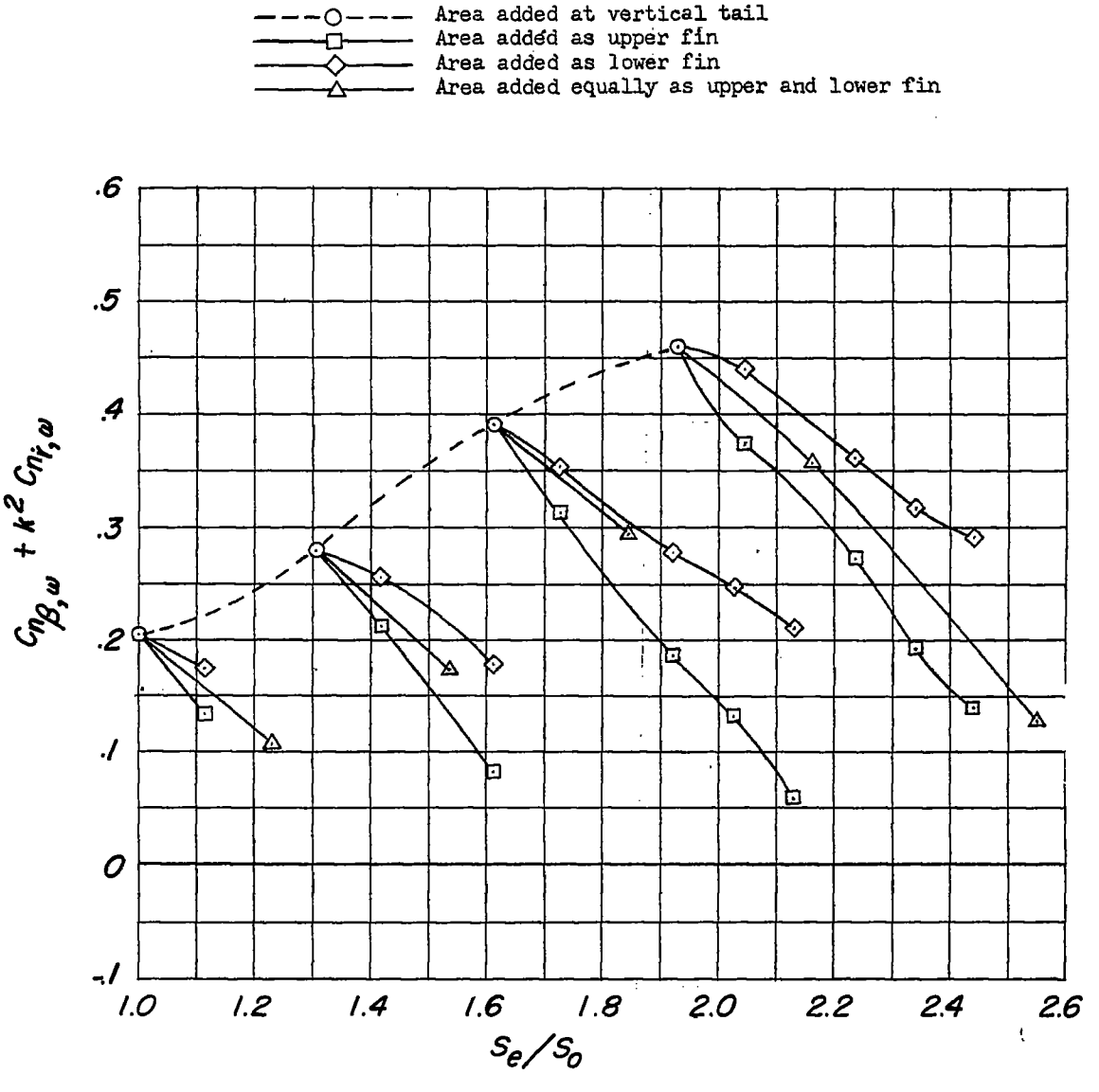

(a) $\alpha = 0^\circ$.

Figure 18.- Variation of $C_{n_{\beta,\omega}} + k^2 C_{n_{\dot{r},\omega}}$ with exposed vertical tail and fin area as measured in oscillation tests.

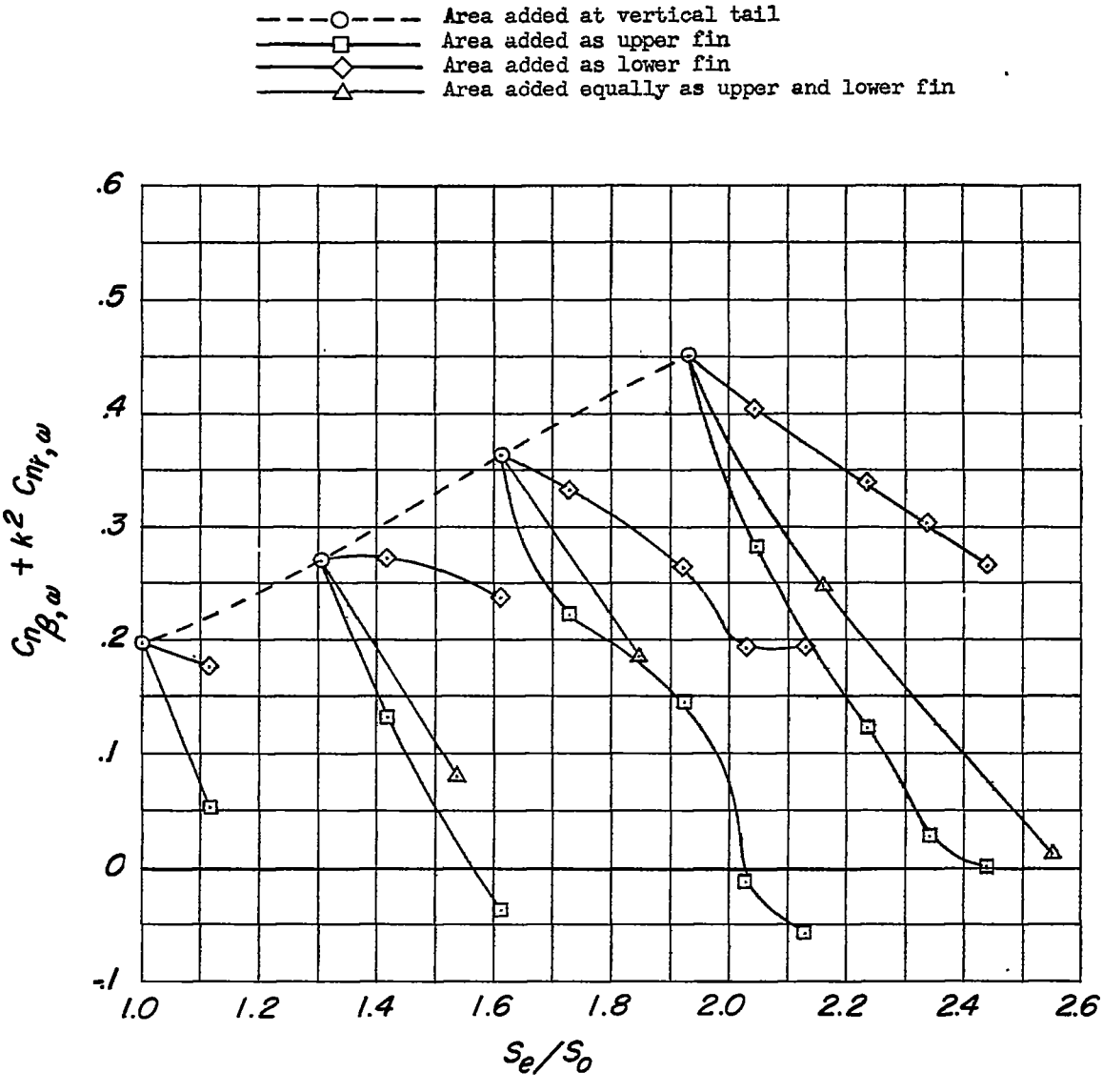

(b) $\alpha = 6^\circ$.

Figure 18.- Continued.

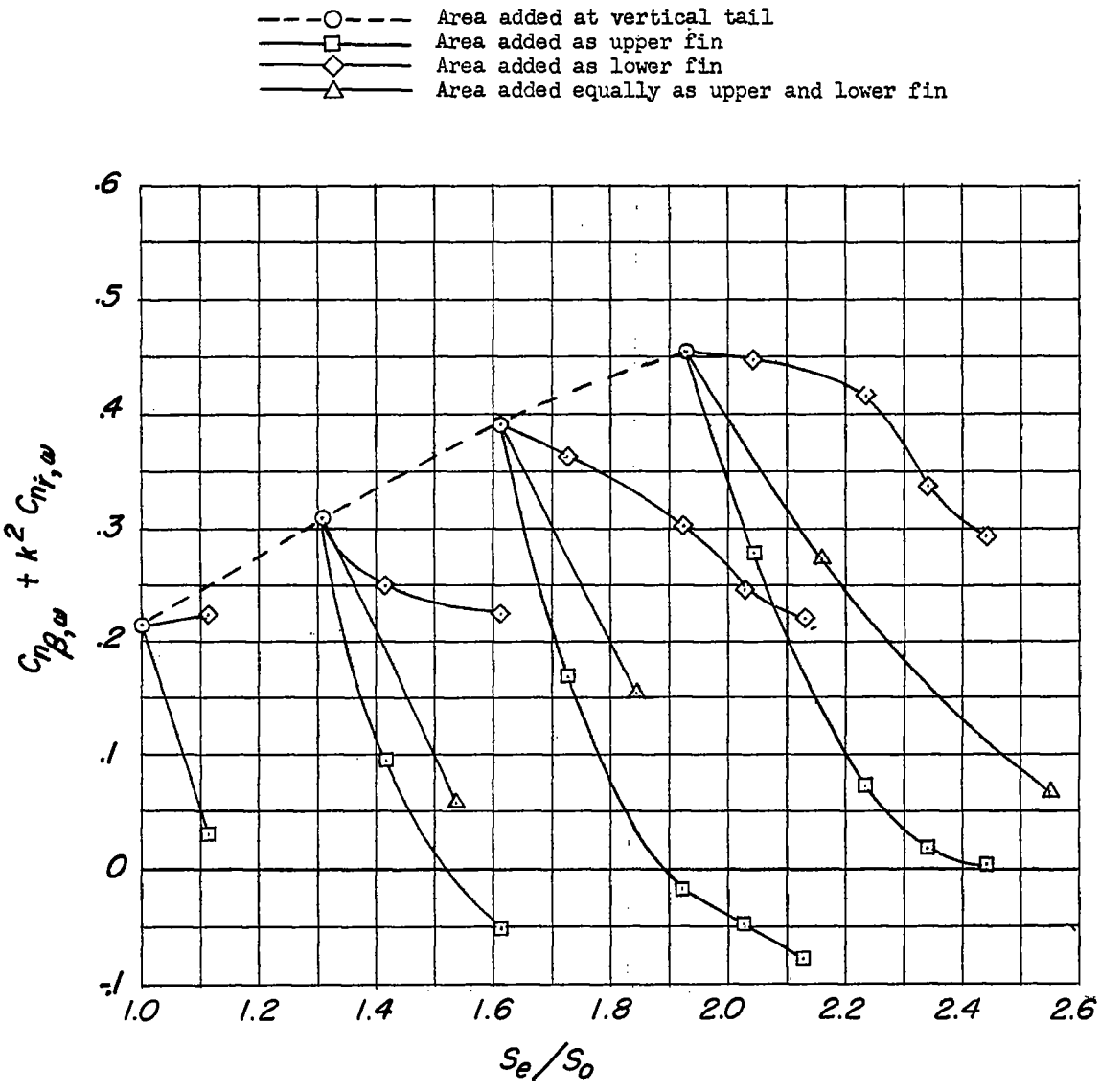

(c) $\alpha = 12^\circ$.

Figure 18.- Concluded.

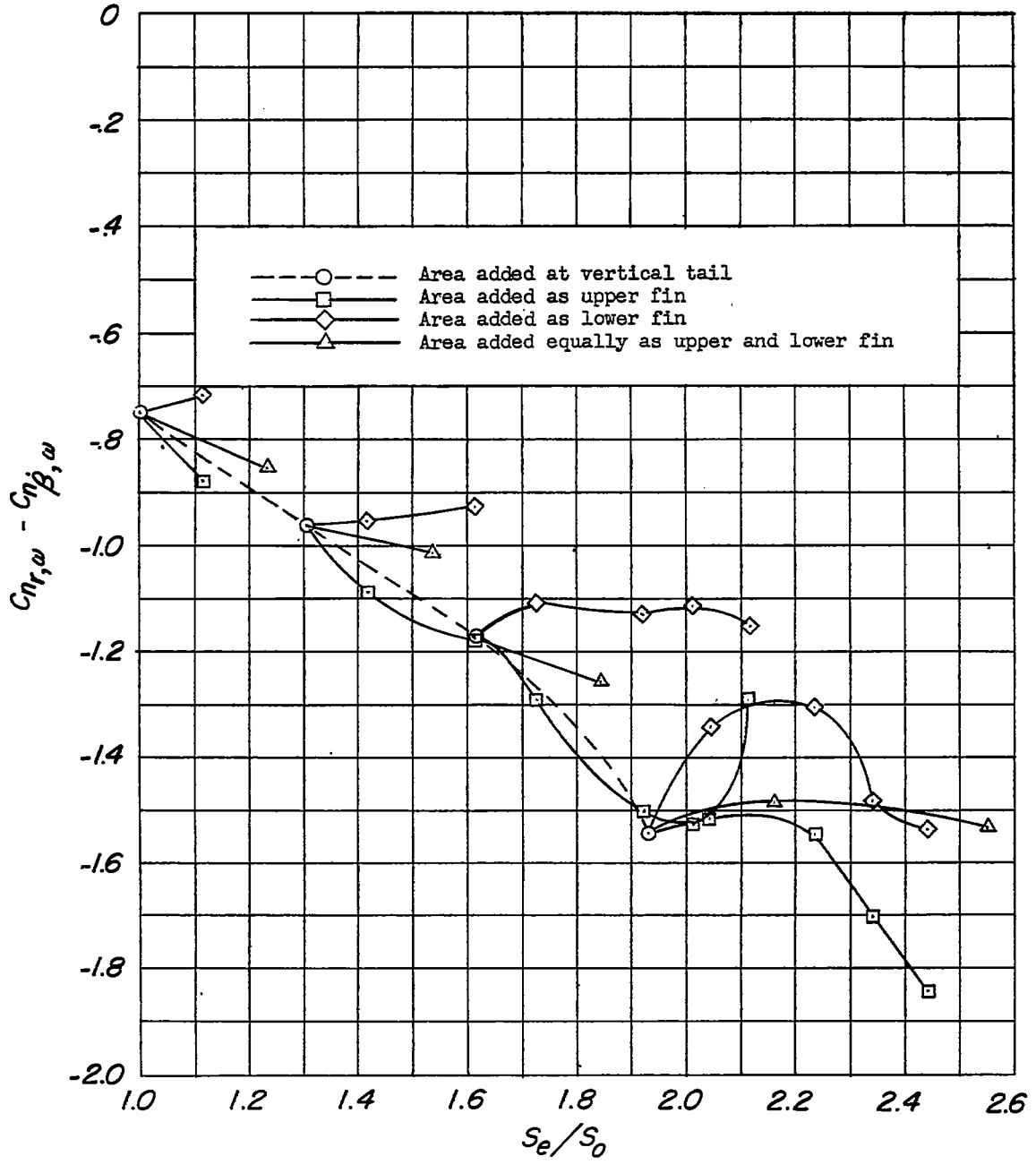

(a) $\alpha = 0^\circ$.

Figure 19.- Variation of $C_{n_{r,\omega}} - C_{n_{\dot{\beta},\omega}}$ with exposed vertical tail and fin area as measured in oscillation tests.

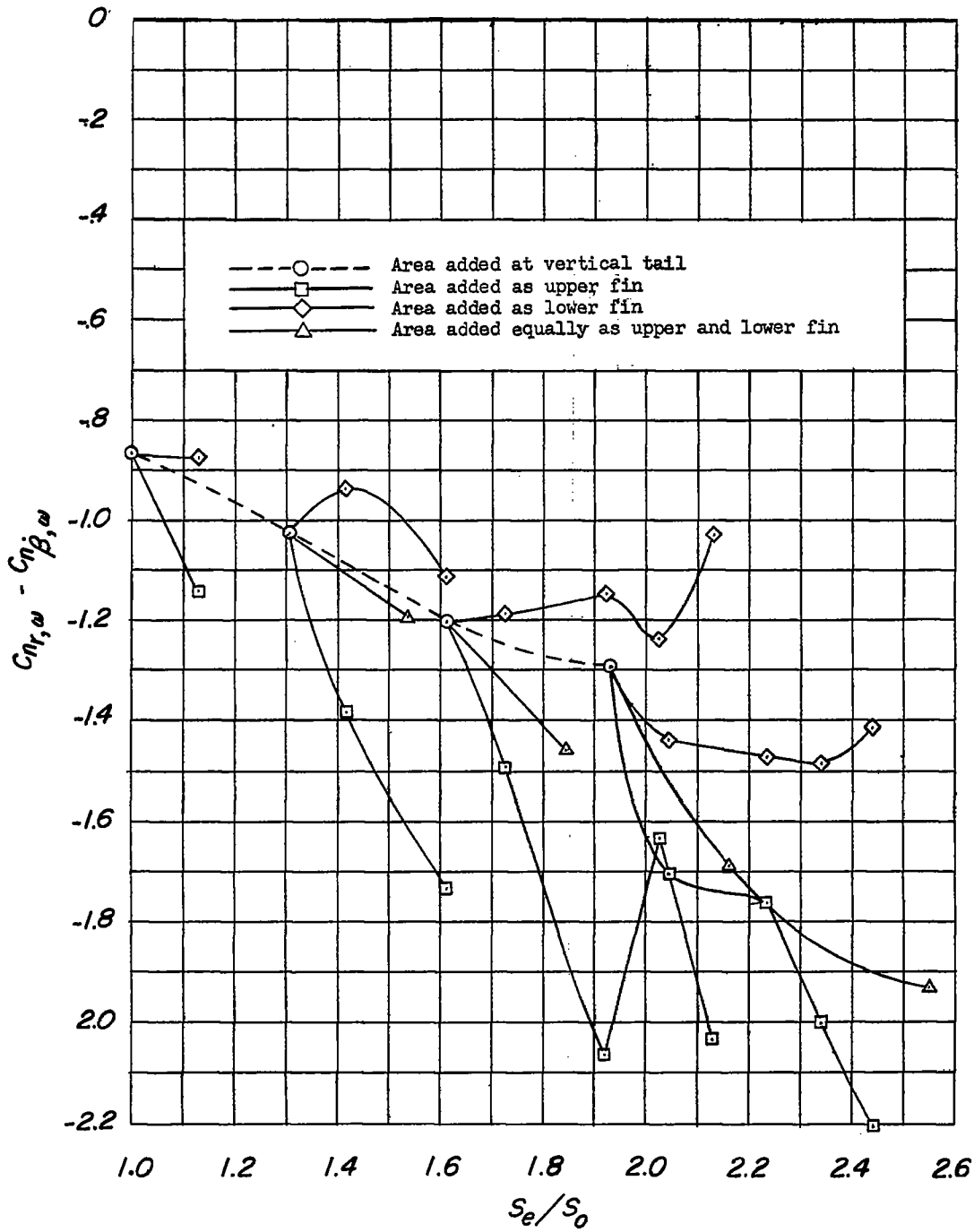

(b) $\alpha = 6.4^\circ$.

Figure 19.- Continued.

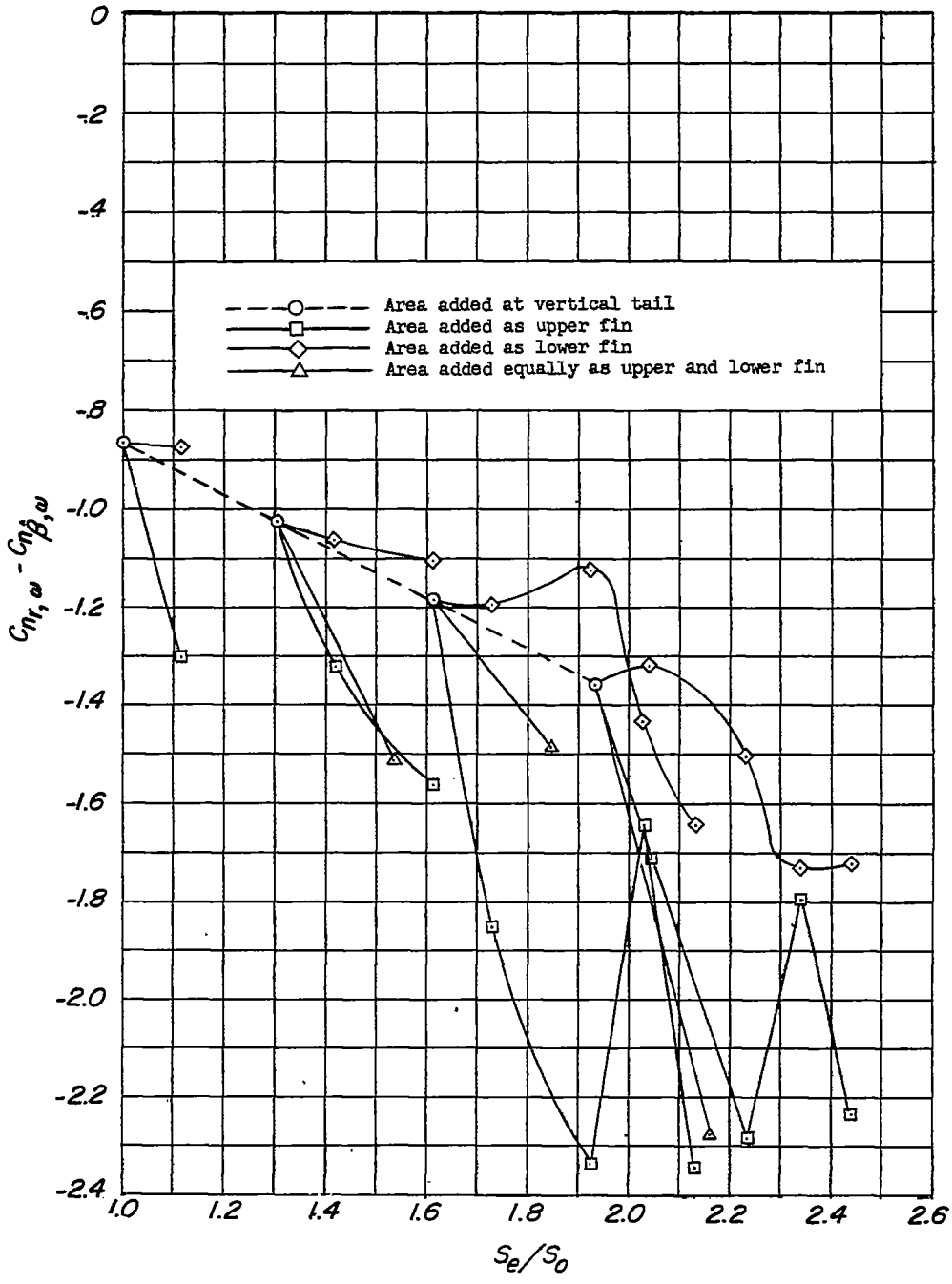

(c) $\alpha = 12.6^{\circ}$.

Figure 19.- Concluded.

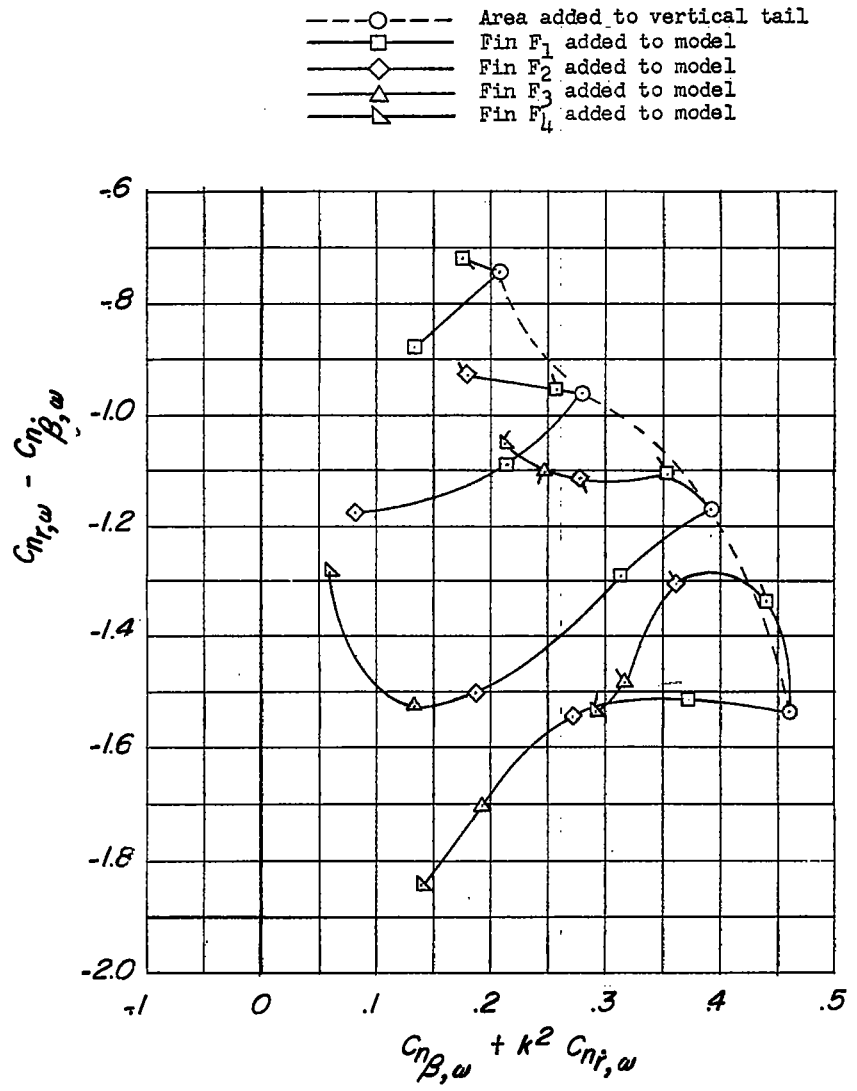

(a) $\alpha = 0^\circ$.

Figure 20.- Values of $C_{n_{r,\omega}} - C_{n_{\dot{\beta},\omega}}$ and $C_{n_{\beta,\omega}} + k^2 C_{n_{\dot{r},\omega}}$ for the various model configurations. Unflagged symbols indicate upper fin; flagged symbols indicate lower fin.

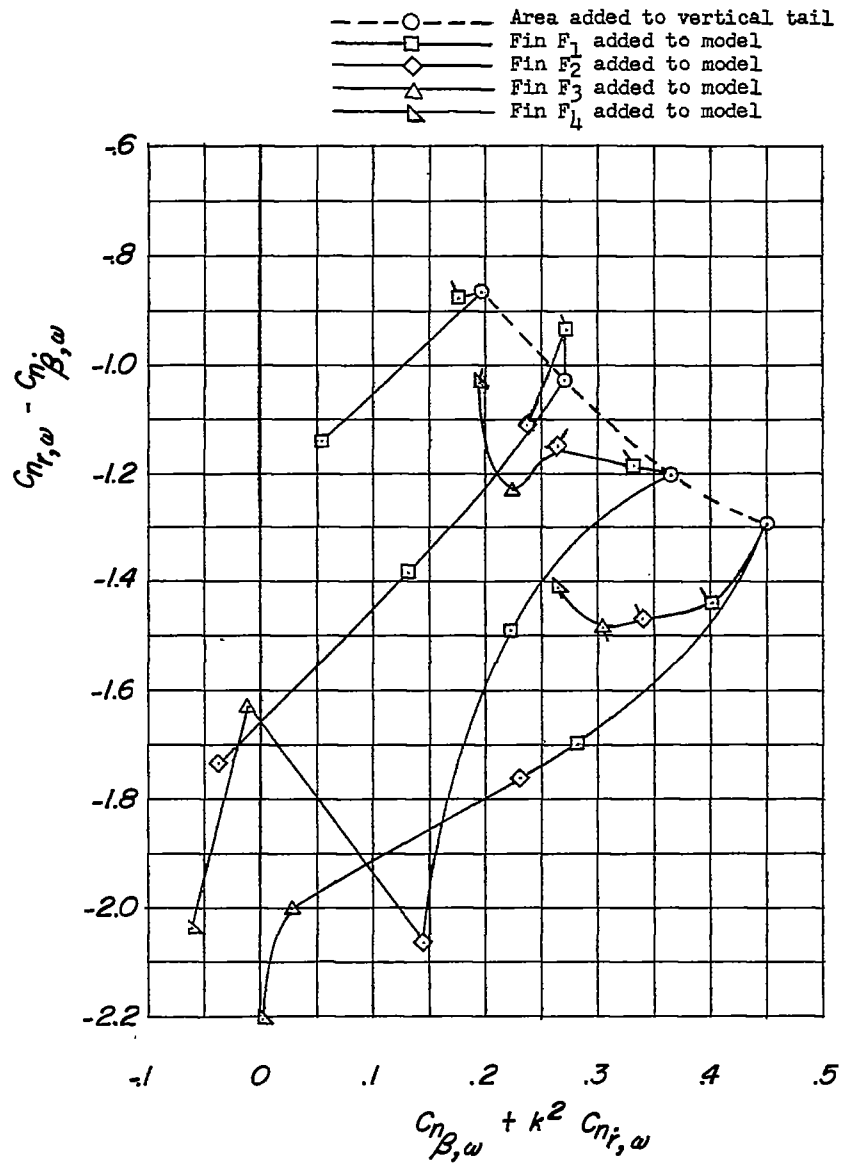

(b) $\alpha = 6.4^\circ$.

Figure 20.- Continued.

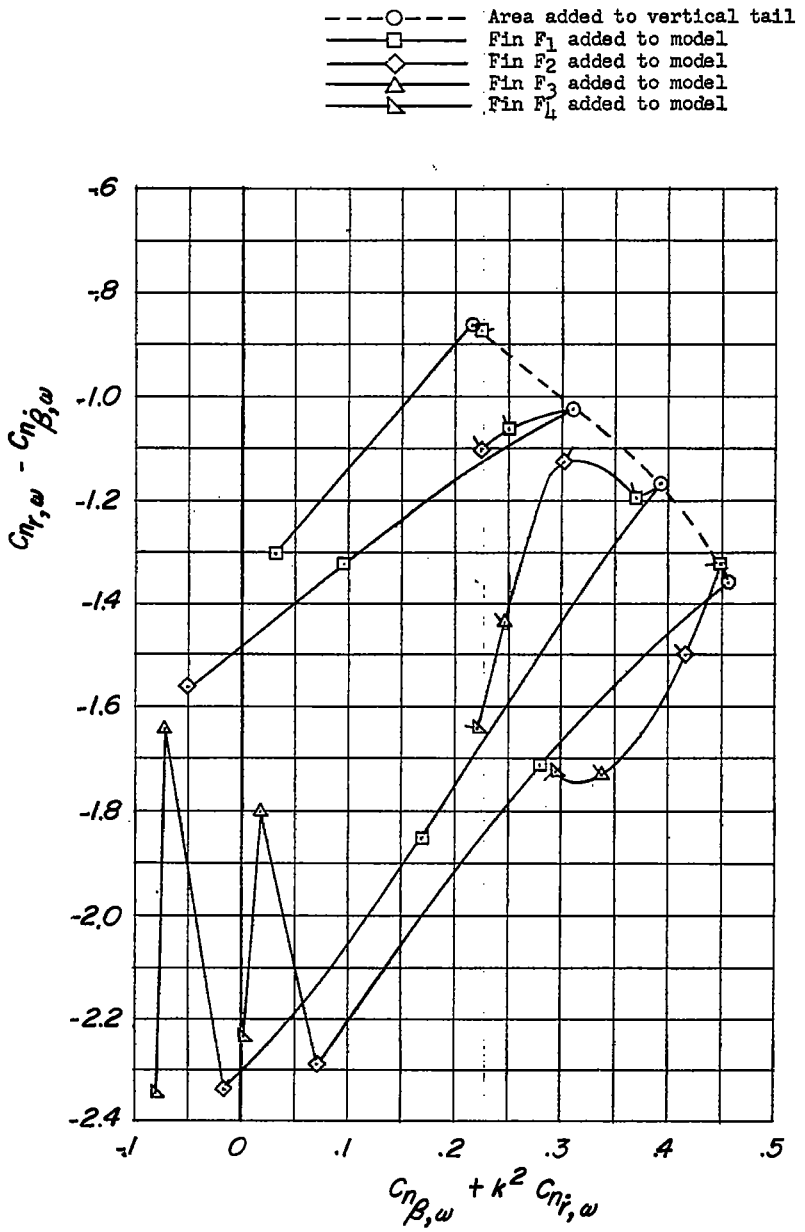

(c) $\alpha = 12.6^\circ$.

Figure 20.- Concluded.